DTIC FILE COPY

SECURITY CLASSIFICATION OF THIS PAGE

REPORT DOCUMENTATION PAGE

Form Approved
OMB No. 0704-0188

1a. REPORT SECURITY CLASSIFICATION UNCLASSIFIED	1b. RESTRICTIVE MARKINGS NONE
ILE **AD-A217 855** ER(S)	3. DISTRIBUTION/AVAILABILITY OF REPORT APPROVED FOR PUBLIC RELEASE; UNLIMITED DISTRIBUTION
	5. MONITORING ORGANIZATION REPORT NUMBER(S) AFIT/CI/CIA-89-138D
6a. NAME OF PERFORMING ORGANIZATION AFIT STUDENT AT UNIVERSITY OF ILLINOIS	6b. OFFICE SYMBOL (If applicable)
	7a. NAME OF MONITORING ORGANIZATION AFIT/CIA
6c. ADDRESS (City, State, and ZIP Code)	7b. ADDRESS (City, State, and ZIP Code) Wright-Patterson AFB OH 45433-6583
8a. NAME OF FUNDING/SPONSORING ORGANIZATION	8b. OFFICE SYMBOL (If applicable)
	9. PROCUREMENT INSTRUMENT IDENTIFICATION NUMBER
8c. ADDRESS (City, State, and ZIP Code)	10. SOURCE OF FUNDING NUMBERS

PROGRAM ELEMENT NO.	PROJECT NO.	TASK NO.	WORK UNIT ACCESSION NO.

11. TITLE (Include Security Classification) (UNCLASSIFIED)
Investigation of Tapered Multiple Microstrip Lines for VLSI Circuits

12. PERSONAL AUTHOR(S)
Mark Andrew Mehalic

13a. TYPE OF REPORT	13b. TIME COVERED	14. DATE OF REPORT (Year, Month, Day)	15. PAGE COUNT
DISSERTATION	FROM _____ TO _____	1989	74

16. SUPPLEMENTARY NOTATION
APPROVED FOR PUBLIC RELEASE IAW AFR 190-1
ERNEST A. HAYGOOD, 1st Lt, USAF
Executive Officer, Civilian Institution Programs

17. COSATI CODES			18. SUBJECT TERMS (Continue on reverse if necessary and identify by block number)
FIELD	GROUP	SUB-GROUP	

19. ABSTRACT (Continue on reverse if necessary and identify by block number)

DTIC
ELECTE
FEB 12 1990
S D
D

20. DISTRIBUTION/AVAILABILITY OF ABSTRACT	21. ABSTRACT SECURITY CLASSIFICATION
XX UNCLASSIFIED/UNLIMITED ☐ SAME AS RPT. ☐ DTIC USERS	UNCLASSIFIED

22a. NAME OF RESPONSIBLE INDIVIDUAL	22b. TELEPHONE (Include Area Code)	22c. OFFICE SYMBOL
ERNEST A. HAYGOOD, 1st Lt, USAF	513-255-2259	AFIT/CI

DD Form 1473, JUN 86 *Previous editions are obsolete.* SECURITY CLASSIFICATION OF THIS PAGE

INVESTIGATION OF TAPERED MULTIPLE MICROSTRIP LINES FOR VLSI CIRCUITS

Mark Andrew Mehalic, Captain, USAF
Ph. D. Dissertation (74 pages)
Department of Electrical and Computer Engineering
University of Illinois at Urbana-Champaign, 1989

Tapered, coupled, microstrip transmission lines are an increasingly important part of high-speed digital circuits. These lines, used as interconnects between integrated circuit devices, are modeled using an iteration-perturbation approach applied in the spatial domain. The approach is used first to solve the static problem, and then to iterate on the static solution to obtain the charge and current distributions on the lines at different frequencies. From this model, a frequency-dependent scattering parameter characterization is determined. Results for typical geometries are presented and are compared with those published by other authors.

A time-domain simulation of pulse propagation through the tapered, coupled, microstrip lines is performed. The frequency-domain scattering parameters are inverse Fourier transformed to obtain the time-domain Green's function. The input pulse is convolved with the Green's function, and a Newton-Raphson algorithm is applied to account for nonlinear loads. Good agreement is found with other published results.

Finally, some experimental results are shown and an equivalent circuit is proposed. The experimental results verify the model, while the equivalent circuit allows the time-domain simulation to be performed in less time with a negligible loss in accuracy. Results show that the equivalent circuit gives essentially the same time-domain response in about one-tenth of the simulation time. Theses.(RH)

A

90 02 12 037

INVESTIGATION OF TAPERED MULTIPLE MICROSTRIP LINES FOR VLSI CIRCUITS

BY

MARK ANDREW MEHALIC

B. S., Pennsylvania State University, 1980
M. S., Air Force Institute of Technology, 1983

THESIS

Submitted in partial fulfillment of the requirements
for the degree of Doctor of Philosophy in Electrical Engineering
in the Graduate College of the
University of Illinois at Urbana-Champaign, 1989

Accesion For
NTIS CRA&I
DTIC TAB
Unannounced
Justification
By
Distribution /
Availability Codes
Dist | Avail and / or Special
A-1

Urbana, Illinois

UNIVERSITY OF ILLINOIS AT URBANA-CHAMPAIGN

THE GRADUATE COLLEGE

AUGUST 1989

WE HEREBY RECOMMEND THAT THE THESIS BY

MARK ANDREW MEHALIC

ENTITLED INVESTIGATION OF TAPERED

MULTIPLE MICROSTRIP LINES FOR VLSI CIRCUITS

BE ACCEPTED IN PARTIAL FULFILLMENT OF THE REQUIREMENTS FOR

THE DEGREE OF DOCTOR OF PHILOSOPHY

R. Mittra
Director of Thesis Research

Timothy N. Trick
Head of Department

Committee on Final Examination†

R. Mittra
Chairperson

B. T. Kang

Paul E. Mayes

† Required for doctor's degree but not for master's.

O-517

ABSTRACT

Tapered, coupled, microstrip transmission lines are an increasingly important part of high-speed digital circuits. These lines, used as interconnects between integrated circuit devices, are modeled using an iteration-perturbation approach applied in the spatial domain. The approach is used first to solve the static problem, and then to iterate on the static solution to obtain the charge and current distributions on the lines at different frequencies. From this model, a frequency-dependent scattering parameter characterization is determined. Results for typical geometries are presented and are compared with those published by other authors.

A time-domain simulation of pulse propagation through the tapered, coupled, microstrip lines is performed. The frequency-domain scattering parameters are inverse Fourier transformed to obtain the time-domain Green's function. The input pulse is convolved with the Green's function, and a Newton-Raphson algorithm is applied to account for nonlinear loads. Good agreement is found with other published results.

Finally, some experimental results are shown and an equivalent circuit is proposed. The experimental results verify the model, while the equivalent circuit allows the time-domain simulation to be performed in less time with a negligible loss in accuracy. Results show that the equivalent circuit gives essentially the same time-domain response in about one-tenth of the simulation time.

DEDICATION

To my wife Linda and my son
Nicholas, both of whom
became a part of my life
during my time at the
University.

ACKNOWLEDGEMENTS

I would like to thank my advisor, Professor Raj Mittra, for his support and guidance in this research. I would also like to thank Dr. Jose Schutt-Aine and Mr. Paul Aoyagi for their assistance in obtaining the experimental results. Thanks also go to Dr. Chi Chan, whose keen eye and tenacious mind helped me find and remove the errors in my theory and computer program. Finally, I am grateful to the members of the Electromagnetic Communication Laboratory and the Electromagnetics Laboratory, whose friendship and camaraderie made the task bearable.

TABLE OF CONTENTS

CHAPTER	PAGE
1. INTRODUCTION	1
2. MODELING OF A SINGLE TAPERED MICROSTRIP LINE	3
2.1. Introduction	3
2.2. Theory	4
2.2.1. Quasi-static ε_{eff} and Z_0 calculations	6
2.2.2. Frequency-dependent ε_{eff} and Z_0 calculations	10
2.2.3. Scattering parameter determination	14
2.3. Results	14
2.3.1. Uniform line results	15
2.3.2. Tapered line results	17
2.4. Conclusions	20
3. MODELING OF MULTIPLE TAPERED MICROSTRIP LINES	22
3.1. Introduction	22
3.2. Theory	23
3.2.1. Quasi-static solution	25
3.2.2. Frequency-dependent solution	28
3.2.3. Correction for finite thickness	29
3.2.4. Line losses	30
3.2.5. Scattering parameter determination	34
3.3. Results	35
3.3.1. Uniform line results	35
3.3.2. Tapered line results	35
3.4. Conclusions	41
4. TIME-DOMAIN SIMULATION OF MULTIPLE TAPERED MICROSTRIP LINES	42
4.1. Introduction	42
4.2. Theory	43
4.3. Results	45
4.4. Conclusions	47

5. EXPERIMENTAL CHARACTERIZATION OF MULTIPLE TAPERED MICROSTRIP LINES 50
5.1. Introduction 50
5.2. Test Procedures 50
5.3. Results 51
5.4. Conclusions 57
6. EQUIVALENT CIRCUIT CHARACTERIZATION 58
6.1. Introduction 58
6.2. Model Development 59
6.3. Results 61
6.4. Conclusions 66
7. CONCLUSIONS 69
REFERENCES 70
VITA 74

CHAPTER 1.

INTRODUCTION

The modeling and analysis of signal interconnects in high-speed digital circuits have become more complicated in recent years. As the clock rates of digital circuits become faster, the frequency of operation increases and the rise time of the digital gating pulses shortens. Currently, digital devices can achieve rise times of less than 1 nanosecond (nsec), with 40 picoseconds (psec) not unreasonable. Digital signals with sharp rise times and short durations contain significant frequency components from several gigahertz up to 10 gigahertz (GHz). For frequencies above a few gigahertz, the lumped circuit approximations commonly used as models for interconnects in digital circuits can lead to erroneous results. The distance the signal must travel in terms of a wavelength is large enough that lumped-element approximations are no longer valid, and thus the interconnect must be treated as a transmission line. In addition, as frequencies get higher, parameters normally considered constant, such as the effective dielectric constant, become a function of frequency. This results in different propagation velocities for different frequency components, leading to dispersion and distortion of the propagated pulse. An additional complication comes from the fact that interconnects typically contain some type of discontinuity, causing reflections of the incident pulse. The discontinuity could be a bend, a via, or, as in this study, a taper in the line. Furthermore, an increase in packing density results in lines being closer together, giving rise to undesired coupling. Finally, the terminations for the interconnection could be nonlinear active devices.

Currently, no unified study of all these complications has been undertaken. Other authors have investigated various parts of the problem. For example, dispersion in microstrip lines has typically been analyzed using the spectral domain technique [1] - [3]. Kretch and Collin [4], on the other hand, investigated the frequency-dependent parameters for a single uniform microstrip line using an iteration-perturbation approach in the spatial domain. Rao et al. had written a program to characterize a linear taper, but only using a static approach [5]. Syahkal and Davies [6] extended the spectral-domain approach to tapered lines. However, their formulation does not include losses. The possibility of crosstalk upsetting logic states in coupled lines was investigated by Smith and Snyder [7]. Ghione et al. [8] combined the analysis of uniform lines by the spectral-domain technique

with a time-domain analysis of pulse propagation. But the analysis was limited to linear terminations and to lines whose lengths were less than the wavelength of the signal. However, these techniques are not easy to combine with other programs, especially circuit simulators. Only recently, Romeo and Santomauro have integrated a uniform, coupled, lossless set of transmission lines into the SPICE circuit simulator [9].

This thesis investigates the effects of tapered, coupled, microstrip lines used as interconnects in high-speed digital circuits. Effects such as conductor loss and conductor thickness are included. An important concern is the use of nonlinear terminations. The nonlinearity is usually due to the load being an active device. Many active devices have the input modeled by a capacitor and a diode in parallel. The effects of the change in effective dielectric constant due to frequency and of a transverse current on the scattering parameters of the interconnects are also evaluated.

Each chapter of this thesis covers a different aspect of the problem. A single-line taper is modeled and a method for determining the scattering parameters (S-parameters) is derived in Chapter 2. The method uses an integral-equation approach based on the Green's function of the structure. An iterative scheme derived from potential theory is added to evaluate the effects of frequency on the S-parameters. In Chapter 3, the previous model is extended to the multiline case. The effects of conductor loss and conductor thickness are added. In this thesis, only the three-line structure is considered. Extensions of the theory to any number of lines is possible, but the numerical calculations become time-consuming. In Chapter 4, a time-domain simulation of the pulse propagating through a three-line tapered structure is performed, using both linear and nonlinear terminations. The amount of crosstalk is evaluated. In Chapter 5, the frequency-domain scattering parameter results are compared to experimental measurements. In Chapter 6, an equivalent circuit for the single-line taper is derived, and its accuracy compared to the full simulation. Conclusions are summarized in Chapter 7.

CHAPTER 2.

MODELING OF A SINGLE TAPERED MICROSTRIP LINE

2.1. Introduction

In this chapter, a method for determining the characteristics of a single tapered microstrip transmission line is developed. The tapered transmission line can be characterized by first separating it into many uniform lines and calculating the effective dielectric constant (ε_{eff}) and characteristic impedance (Z_0) values of the uniform lines. The ε_{eff} and Z_0 values include dispersion effects caused by the transverse current in the transmission line and, thus, are a function of frequency. Throughout this thesis, this condition will be called frequency-dependent, and does not imply a full-wave analysis. An iteration-perturbation technique is used which first finds a static solution and then determines a correction to that solution to account for dispersion effects. The S-parameters are determined for the uniform sections and are cascaded to determine the S-parameters for the tapered line. Results are presented for both a uniform line and a tapered line, with comparisons made to published results and to results from a commercial computer-aided design package.

Several authors have characterized uniform lines, including dispersion effects [10] - [13]. Most methods of including dispersion for a single uniform line consist of an empirical formula that defines the effective dielectric constant and characteristic impedance as functions of frequency. However, these empirical methods cannot be applied directly to tapered lines. Goossen and Hammond [13] use a quasi-transverse electromagnetic (TEM) approximation that is valid only up to the lowest frequency where non-TEM modes can propagate. The concept of characterizing a tapered line by dividing it into many small uniform lines has been shown to be valid. Rao et al. [5] present a method for calculating characteristics of a single tapered line by dividing the line into many uniform sections. However, their approach uses a static TEM approximation and thus does not include dispersion. The concept of cascading sections using generalized scattering parameters was described by Chu and Itoh [14] and can be applied to any geometry. The analysis was based on the use of the equivalent waveguide model for microstrip lines.

Section 2.2 presents the quasi-static and frequency-dependent theory development. The theory uses an efficient iteration-perturbation technique in the spatial domain. In addition, the procedure for cascading uniform sections to form a tapered line is described. The result is an S-parameter characterization of a tapered microstrip line, including dispersion effects. In Section 2.3, the results of the method are presented and compared with results from other methods and authors. Section 2.3.1 presents the uniform line results, while Section 2.3.2 presents the tapered line results. Even though the uniform lines have been thoroughly studied by others, the results are presented to show the consistency of this method with other approaches, such as the spectral domain technique or empirical formulas. The S-parameters for a tapered line are given as a function of frequency. The difference between the quasi-static S-parameters and the frequency-dependent S-parameters is highlighted. Section 2.4 contains the summary and conclusions.

2.2. Theory

This section presents the development of the quasi-static and frequency-dependent theory for calculating the ε_{eff} and Z_0 values and cascading uniform sections to form a tapered line, which is approximated by dividing it into many uniform sections, as shown in Figure 2.1. A cross-sectional diagram of a typical uniform section, including coordinate axes, is shown in Figure 2.2. Each uniform section is analyzed individually to obtain the charge and current distributions using the integral equation formulation in the spatial domain. From the total charge and total current, the effective dielectric constant and characteristic impedance can be found for each section.

Briefly, the procedure is as follows. The integral equations involving the charge or current distributions, Green's functions, and potentials are determined. They are then converted to matrix equations by using point matching. The equations are solved to determine the total charge and total current. Once the total charge and total current are found, the impedance and S-parameters can be calculated. The uniform sections are combined by cascading S-parameters to give an S-parameter representation for the tapered line. To include frequency dependence, a correction term for the potential distribution is found, and the ε_{eff} and Z_0 values are calculated again. The process is repeated until the values converge.

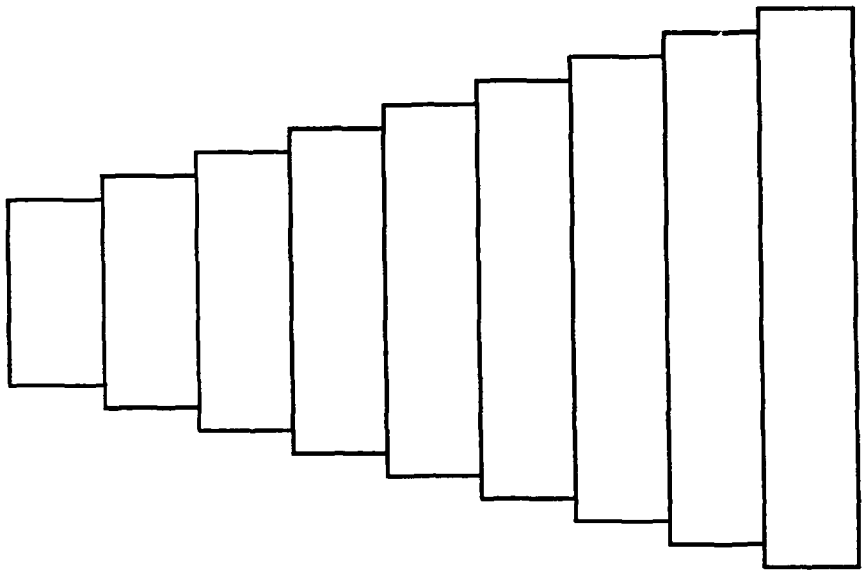

Figure 2.1. Approximation of tapered line by cascading uniform sections.

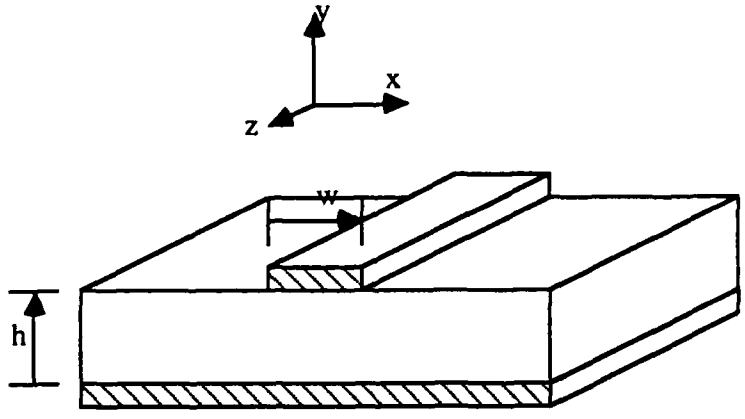

Figure 2.2. Cross section of a typical uniform section of a tapered line.

Section 2.2.1 describes the static calculation of the ε_{eff} and Z_0 values. The integral equations are derived and then converted into matrix equations. Section 2.2.2 describes the iterative technique applied to the quasi-static solution to obtain the frequency-dependent ε_{eff} and Z_0 values. Finally, Section 2.2.3 describes the calculation and cascading of the S-parameters.

2.2.1. Quasi-static ε_{eff} and Z_0 calculations

The single-line taper is analyzed by first dividing it into small sections and approximating each section as being uniform. Then the charge and current distributions can be calculated for each section using a Green's function method-of-moments approach [4]. Once the charge and current distributions are found, the total charge and total current can be determined. Since the potentials are known, the effective dielectric constant ε_{eff} and characteristic impedance Z_0 can be found.

Using the Green's function, the integral equations to be solved are [4]

$$\int_{-\infty}^{\infty} G_1^0(x,x')J_z(x')dx' = \frac{A(x)}{\mu_0}, \tag{2.1}$$

$$\int_{-\infty}^{\infty} G_2^0(x,x')\rho_z(x')dx' = \varepsilon_0\,\phi(x)\,, \tag{2.2}$$

where for the quasi-static case, $\varepsilon_0\phi(x) = 1$ and $A(x)/\mu_0 = 1$. The Green's functions are given by

$$G_1^0 = -\frac{1}{4\pi}\ln|x^2 - x'^2| + \frac{1}{8\pi}\ln|[(2a)^2 + (x+x')^2][(2a)^2 + (x-x')^2]|, \text{ and} \tag{2.3}$$

$$G_2^0 = \frac{2}{\kappa_g+1}G_1^0 + \frac{-\kappa_g}{2\pi(\kappa_g+1)^2}\left(\frac{\kappa_g-1}{2\kappa_g}\ln\frac{\cosh\frac{\pi\alpha}{a} + \cos\frac{\pi\alpha}{2a}(x-x')}{\cosh\frac{\pi\alpha}{a} - \cos\frac{\pi\alpha}{2a}(x-x')}\,\frac{\cosh\frac{\pi\alpha}{a} + \cos\frac{\pi\alpha}{2a}(x+x')}{\cosh\frac{\pi\alpha}{a} - \cos\frac{\pi\alpha}{2a}(x+x')}\right)$$

$$+\sum_{m=1}^{\infty}(-\eta)^m \ln \frac{\cosh(m+1)\frac{\pi\alpha}{a}+\cos\frac{\pi\alpha}{2a}(x-x')}{\cosh(m+1)\frac{\pi\alpha}{a}-\cos\frac{\pi\alpha}{2a}(x-x')}\,\frac{\cosh(m+1)\frac{\pi\alpha}{a}+\cos\frac{\pi\alpha}{2a}(x+x')}{\cosh(m+1)\frac{\pi\alpha}{a}-\cos\frac{\pi\alpha}{2a}(x+x')} . \tag{2.4}$$

The integrals become finite because J_z and ρ_z are nonzero only on the conductor. Note that only the even part of the Green's function needs to be included for the single-line case.

Next, expand J_z and ρ_z in terms of their basis functions. Thus,

$$J_z(x') = I_0B_0(x') - I_1B_2(x') + I_2B_4(x') - I_3B_6(x') , \tag{2.5}$$

$$\rho_z(x') = Q_0B_0(x') - Q_1B_2(x') + Q_2B_4(x') - Q_3B_6(x') , \tag{2.6}$$

where the basis functions were chosen as

$$B_i(x') = \frac{T_i(x')}{\sqrt{1 - x'^2}} . \tag{2.7}$$

$T_i(x')$ is the i^{th} Chebyshev polynomial. A plot of the four basis functions is shown in Figure 2.3. Note that these are entire-domain basis functions with the appropriate edge singularity already included in each basis function. Only even basis functions are required due to the fact that the distributions on the single strip are even.

Inserting Equations (2.3) and (2.6) into Equations (2.1) and (2.2) and normalizing so that the width of the strip extends from -1 to 1 give

$$\int_{-1}^{1} G_1^0(x,x') \left(I_0B_0(x')-I_1B_2(x')+I_2B_4(x')-I_3B_6(x')\right) dx' = 1 , \tag{2.8}$$

$$\int_{-1}^{1} G_2^0(x,x') \left(Q_0B_0(x')-Q_1B_2(x')+Q_2B_4(x')-Q_3B_6(x')\right) dx' = 1 . \tag{2.9}$$

Now, applying delta testing functions to Equation (2.8), where x_i is the point at which the equation is enforced, gives

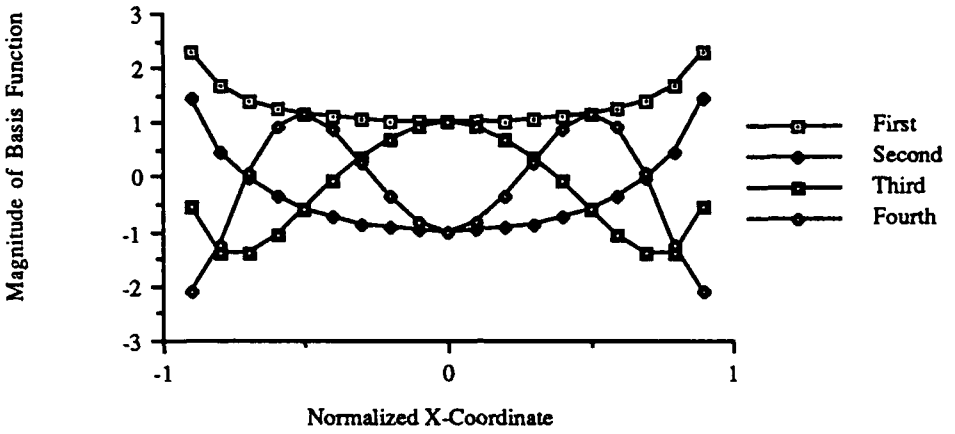

Figure 2.3. Four basis functions used for current and charge expansion.

$$\int_{-1}^{1} \delta(x_i) \int_{-1}^{1} G_1{}^0(x,x')[\sum I_j B_j(x')]dx'dx = \int \delta(x_i)dx \, . \qquad (2.10)$$

Thus, the integral equation can be converted into a matrix equation as follows:

$$\int_{-1}^{1} G_1{}^0(x_i,x')[\sum I_j B_j(x')]dx' = \delta(x_i) = 1 \, ; \qquad (2.11)$$

$$\sum I_j \int_{-1}^{1} G_1{}^0(x_i,x')B_j(x')dx' = 1 \, . \qquad (2.12)$$

The matrix equation is

$$\begin{bmatrix} a(0,0) & a(0,1) & a(0,2) & a(0,3) \\ a(1,0) & a(1,1) & a(1,2) & a(1,3) \\ a(2,0) & a(2,1) & a(2,2) & a(2,3) \\ a(3,0) & a(3,1) & a(3,2) & a(3,3) \end{bmatrix} \begin{bmatrix} I_0 \\ I_1 \\ I_2 \\ I_3 \end{bmatrix} = \frac{1}{\mu_0} \begin{bmatrix} A(x_0) \\ A(x_1) \\ A(x_2) \\ A(x_3) \end{bmatrix} = \begin{bmatrix} 1 \\ 1 \\ 1 \\ 1 \end{bmatrix}, \tag{2.13}$$

where the columns correspond to the basis functions and the rows correspond to the field points at which the integral equation is being enforced. The number of basis functions equals the number of field points at which the equation is being enforced; thus, the matrix is square. The matrix elements are

$$a(i,j) = \int_{-1}^{1} G_1{}^0(x_i,x')B_j(x')dx' , \quad i, j = 0, 1, 2, 3 . \tag{2.14}$$

The integration can be accomplished numerically. The element a(i,j) represents the contribution to point i of the j^{th} basis function integrated with the Green's function. Similarly, Equation (2.9) for the charge distribution becomes

$$\begin{bmatrix} a(0,0) & a(0,1) & a(0,2) & a(0,3) \\ a(1,0) & a(1,1) & a(1,2) & a(1,3) \\ a(2,0) & a(2,1) & a(2,2) & a(2,3) \\ a(3,0) & a(3,1) & a(3,2) & a(3,3) \end{bmatrix} \begin{bmatrix} Q_0 \\ Q_1 \\ Q_2 \\ Q_3 \end{bmatrix} = \begin{bmatrix} 1 \\ 1 \\ 1 \\ 1 \end{bmatrix}, \tag{2.15}$$

where the matrix elements are given by

$$a(i,j) = \int_{-1}^{1} G_2{}^0(x_i,x')B_j(x')dx' , \quad i, j = 0, 1, 2, 3 . \tag{2.16}$$

The matrix equation is then solved for the basis function coefficients using Gaussian elimination. From this, the total charge can be found from

$$Q_{total} = \int_{-1}^{1} [Q_0B_0(x') + Q_1B_1(x') + Q_2B_2(x') + Q_3B_3(x')]\, dx' . \tag{2.17}$$

Evaluating each term individually gives

$$\int_{-1}^{1} Q_0B_0(x')\, dx' = \pi\, Q_0 , \tag{2.18}$$

$$\int_{-1}^{1} Q_1B_1(x')\, dx' = 0 , \tag{2.19}$$

$$\int_{-1}^{1} Q_2 B_2(x')\,dx' = 0\,, \tag{2.20}$$

$$\int_{-1}^{1} Q_3 B_3(x')\,dx' = 0\,. \tag{2.21}$$

Thus, $Q_{total} = \pi\, Q_0$. Likewise, $I_{total} = \pi\, I_0$. From the total charge and total current, the effective dielectric constant and characteristic impedance can be found.

$$\varepsilon_{eff} = \frac{Q_{total}}{I_{total}}\,, \tag{2.22}$$

$$Z_0 = \frac{\eta_0}{I_{total}\sqrt{\varepsilon_{eff}}}\,. \tag{2.23}$$

These are the static values used as a starting point for the iteration-perturbation technique described in the next section.

2.2.2. Frequency-dependent ε_{eff} and Z_0 calculations

For the static case, the right-hand sides of Equations (2.1) and (2.2) were constant because the transverse component of the current was assumed to be zero; thus, the potentials were not a function of x. For the frequency-dependent case, however, a transverse component of the current must be considered. Since the exact functional form of the right-hand side is unknown, a perturbation-iteration approach based on potential theory will be used.

First, the quasi-static solution must be found, as done in Section 2.2.1. To include the transverse current $J_x(x)$, use the equation $\overline{E} = -j\omega\overline{A} - \nabla\phi$ and the boundary condition $E_x = 0$ on the conductor to obtain $-j\omega A_x = \frac{\partial\phi}{\partial x}$. Integrating in the x direction give

$$\phi(x,H) = -j\omega\int_{0}^{x} A_x\,dx + \phi(0,H). \tag{2.24}$$

Rearranging, setting $\phi(0,H) = \frac{1}{\varepsilon_0}$, and substituting for A_x give

$$\varepsilon_0 \phi(x,H) = 1 - j\omega\mu_0\varepsilon_0 \int_0^x \int_{-1}^{1} G(x,x')J_x(x')dx'dx \text{ , or} \tag{2.25}$$

$$\varepsilon_0 \phi(x) = 1 + S(x) \tag{2.26}$$

on the conductor. Recall that the strip width has been normalized. The right-hand side is no longer just a constant term, but a constant term with a correction term that depends on the transverse current.

The static solutions for ε_{eff}, $\rho(x')$, and $J(x')$ are used to calculate the correction term to the right-hand side. From (2.25) and (2.26), the correction term S(x) is

$$S(x) = - j\omega\mu_0\varepsilon_0 \int_0^x \int_{-1}^{1} G(x,x')J_x(x')dx'dx, \tag{2.27}$$

where $J_x(x')$ is related to ε_{eff}, $\rho(x')$, and $J_z(x')$ by the continuity equation. The Green's function is the same as in the static case. Integrating the continuity equation $\nabla_s J = -j\omega\rho$, equating Fourier components $\frac{n\pi}{2a} J_{xn} = j\omega\,(\varepsilon_{eff}\, J_{zn} - \rho_n)$, and substituting into Equation (2.27) yield

$$S(x) = \sum_{n\ odd} G_{1n}{}^0 \frac{\cos w_n - 1}{w_n{}^2} (\rho_n - \varepsilon_{eff} J_{zn}), \tag{2.28}$$

where all variables are known, $w_n = \frac{n\pi}{2a}$, and the subscript n indicates the n^{th} Fourier component. The new right-hand side is used to determine new basis function coefficients, and thus a new ε_{eff}. The procedure is repeated until ε_{eff} converges to its frequency-dependent value. From this, the frequency-dependent impedance can be determined.

An additional difficulty caused by this technique is that the Fourier coefficients of the charge and current distributions must be determined. The current and charge can be written in terms of their Fourier components as

$$J_z(x) = \sum_{n\ odd} J_{zn} \cos w_n x \text{ ,} \tag{2.29}$$

$$\rho_z(x) = \sum_{n\ odd} \rho_n \cos w_n x \ , \tag{2.30}$$

where

$$J_{zn} = \frac{2}{a}\int_0^1 J_z(x)\cos w_n x\, dx \qquad n \text{ odd}, \tag{2.31}$$

$$\rho_{zn} = \frac{2}{a}\int_0^1 \rho_z(x)\cos w_n x\, dx \qquad n \text{ odd}. \tag{2.32}$$

Likewise, the potentials can be decomposed as

$$\Phi = \sum_{n\ odd} \Phi_n(y)\cos w_n x \ , \tag{2.33}$$

$$A_z = \sum_{n\ odd} A_{zn}(y)\cos w_n x \ , \tag{2.34}$$

$$A_y = \sum_{n\ odd} A_{yn}(y)\cos w_n x \ , \tag{2.35}$$

$$A_x = \sum_{n\ odd} A_{xn}(y)\sin w_n x \ , \tag{2.36}$$

where $e^{-j\beta z}$ has been suppressed. The propagation coefficients are

$$\gamma_{1n} = \sqrt{\beta^2 - \kappa k_0^2 + w_n^2} \ , \tag{2.37}$$

$$\gamma_{2n} = \sqrt{\frac{\kappa}{\kappa_y}(\beta^2 - \kappa_y k_0^2 + w_n^2)} \ , \tag{2.38}$$

$$\gamma_n = \sqrt{\beta^2 - k_0^2 + w_n^2} \ . \tag{2.39}$$

The equations for Φ and A_y must be solved simultaneously. The solutions are

$$\varepsilon_0\Phi_n(y) = \left(\frac{w_1(n)w_3(n)Sh_3(n)}{w_3(n)Sh_3(n)+\varepsilon_r w_1(n)Ch_3(n)} + \frac{k_0^2 Sh_2(n)}{w_1(n)Sh_2(n)+w_2(n)Ch_2(n)}\right)$$

$$\times \frac{\rho_n}{\beta^2 + w_n^2}, \tag{2.40}$$

$$A_{zn}(y) = \frac{\mu_0 J_{zn} Sh_3(n)}{w_1(n)Sh_2(n) + w_2(n)Ch_2(n)}, \tag{2.41}$$

for n = 1, 2, 3, ... The following notations have been used:

$$w_1(n) = \gamma_n \; ; \; w_2(n) = \gamma_{1n} \; ; \; w_3(n) = \gamma_{2n} \; ; \tag{2.42}$$

$$Sh_i(n) = \sinh w_i(n)y \; ; \; Ch_i(n) = \cosh w_i(n)y \; . \tag{2.43}$$

To obtain results at the first frequency increment, new Green's functions are determined using the quasi-static value of ε_{eff}. The new Green's functions are related to Equations (2.40) and (2.41) and are given by

$$G_{1n} = \frac{A_{zn}(h)}{\mu_0 J_{zn}} \text{ and} \tag{2.44}$$

$$G_{2n} = \frac{\varepsilon_0 \phi_n(h)}{\rho_n} . \tag{2.45}$$

The Fourier components are summed to give the new Green's function. The new equations to be solved instead of Equations (2.1) and (2.2) are

$$\int_{-1}^{1} G_1^0(x,x') J_z(x') dx' = 1 + S(x) \tag{2.46}$$

$$\int_{-1}^{1} G_2^0(x,x') \rho_z(x') dx' = 1 + S(x) \; . \tag{2.47}$$

From this integral equation, a new J_{zn} and ρ_n are determined. From these, new values of I_n and Q_n for this frequency increment are calculated. A new value of ε_{eff} can then be determined. This procedure is repeated until the value for ε_{eff} does not change by more than 0.1%. This value is the final ε_{eff} for this frequency. The procedure then steps to the next frequency and calculates a new S(x) from an extrapolated value of ε_{eff}, and starts iterating all over again. For the single line case, the characteristic impedance can be determined from

$$Z_0 = \frac{120\pi}{I_{total}\sqrt{\varepsilon_{eff}}} \left(1 + \sum_{n=1}^{\infty} \frac{k_0^2 \rho_n}{\varepsilon_{eff} k_0^2 + w_1^2(n)} (A_1 - A_2) \right), \tag{2.48}$$

where

$$A_1 = \frac{\varepsilon_r w_1(n) Sh_3(n)}{w_3(n)[w_3(n)Sh_3(n)+\varepsilon_r w_1(n)Ch_3(n)]}, \quad (2.49)$$

$$A_2 = \frac{Sh_2(n)}{w_1(n)Sh_2(n)+w_2(n)Ch_2(n)}. \quad (2.50)$$

2.2.3. Scattering parameter determination

Once the characteristic impedance of the line has been found, it is then used to determine the reflection and transmission coefficients for that small section, using the given reference Z_0. The coefficients are then rotated through the length of the uniform section. The procedure is repeated for each section, and the overall S-matrix is computed by cascading the individual sections.

The reflection and transmission coefficients are calculated from

$$\Gamma = \frac{Z_L - Z_0}{Z_L + Z_0} e^{-2\gamma d}, \quad (2.51)$$

$$T = \frac{2\sqrt{Z_L Z_0}}{Z_L + Z_0} e^{-2\gamma d}, \quad (2.52)$$

where d is the length of the uniform section of the microstrip line. Once the reflection and transmission coefficients for the uniform sections are found, they can be cascaded to obtain the reflection and transmission coefficients for the tapered line. Sections are cascaded by first calculating

$$Z = Z_0 \frac{1 + \Gamma}{1 - \Gamma}. \quad (2.53)$$

This impedance Z is used as the new load impedance Z_L for the next section. The value of Z_L is substituted into Equations (2.51) and (2.52) along with the characteristic impedance Z_0 of the next section. In this way, overall reflection and transmission coefficients for the single-line taper are determined.

2.3. Results

The theory described in Section 2.2 was programmed into a computer algorithm. The program was used to analyze various uniform and tapered geometries. In this section, results for both the uniform line and the tapered line are presented.

2.3.1. Uniform line results

To confirm the validity of this technique, the characteristics of a uniform line were computed and the results compared with other published results. Figures 2.4 and 2.5 show the effect of frequency on the effective dielectric constant and characteristic impedance, respectively, for a nominal ε_r of 12. For Figure 2.4, the effective dielectric constant approached its nominal value of 12 as the frequency increases. This is as expected, because as the frequency increases, the effect of the fringing fields on the effective dielectric constant decreases. In other words, more of the electric field is concentrated in the dielectric. This can also be seen by noting that for any particular frequency, the effective dielectric constant approached the nominal value as the line width increases. The results for the particular case of $\varepsilon_r = 2$ and w/h = 1 are compared with [4] in Figure 2.6. Agreement is excellent, as it should be, since the techniques are similar.

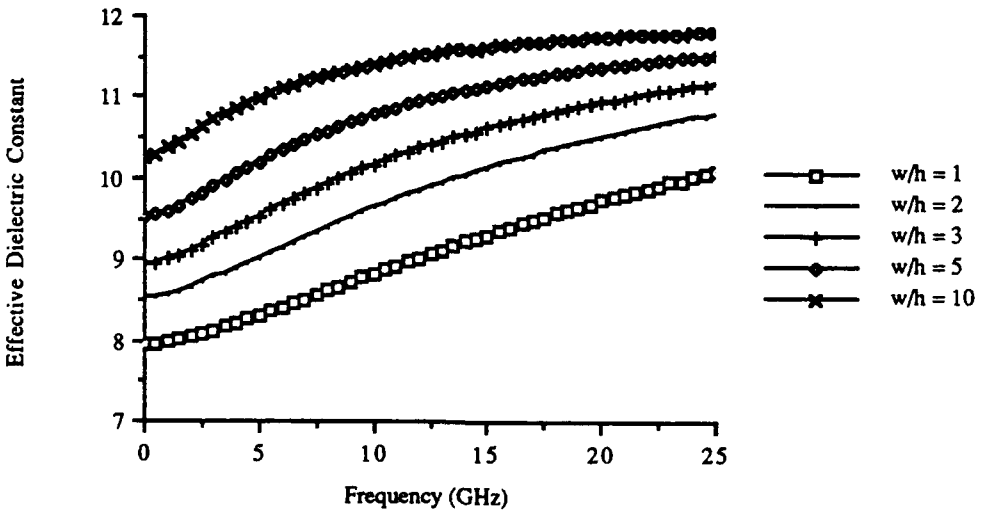

Figure 2.4. Effective dielectric constant as a function of frequency.

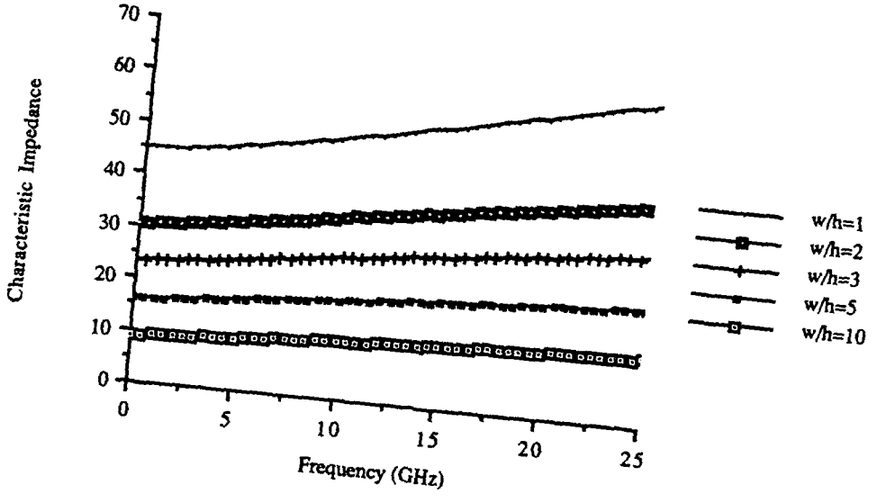

Figure 2.5. Characteristic impedance as a function of frequency.

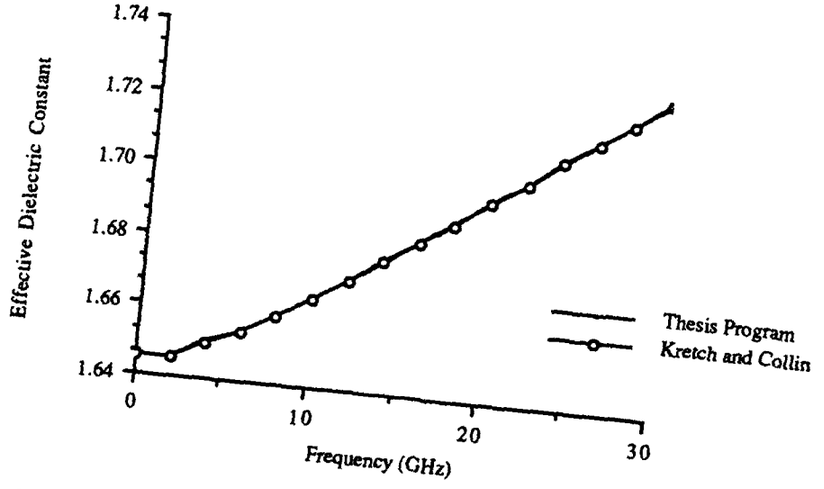

Figure 2.6. Comparison of effective dielectric constant to results of Kretch and Collin [4].

The quasi-static inductance was computed for various w/h ratios and the results compared to those given by Neale and Gopinath [15]. For the worst case of w/h = 0.5, the results differ by about 6%. The comparison is plotted in Figure 2.7.

2.3.2. Tapered line results

The S-parameters generated using this technique were compared with the S-parameters generated by the commercially available program Touchstone by EEsof. The results are for a single line with the parameters given in Table 2.1. The reflection coefficient magnitudes and phases are compared in Figures 2.8 and 2.9, while the transmission coefficient magnitudes are compared in Figures 2.10 and 2.11. As can be seen, the results compare favorably.

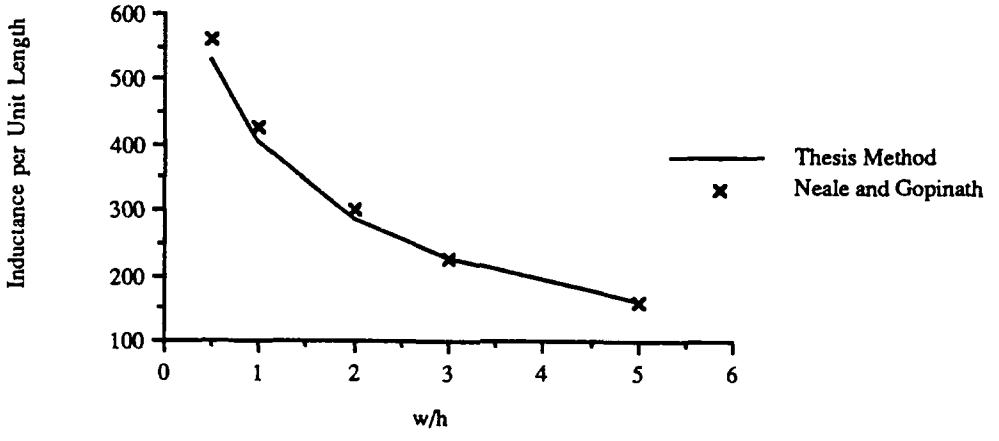

Figure 2.7. Comparison of inductance per unit length from thesis technique with [15].

TABLE 2.1	
PARAMETERS FOR COMPARISON OF THESIS TECHNIQUE WITH TOUCHSTONE	
Width of line at input end	3.0 mm
Width of line at output end	1.0 mm
Length of line	3.0 cm
Relative dielectric constant	2.35
Substrate thickness	1.0 mm

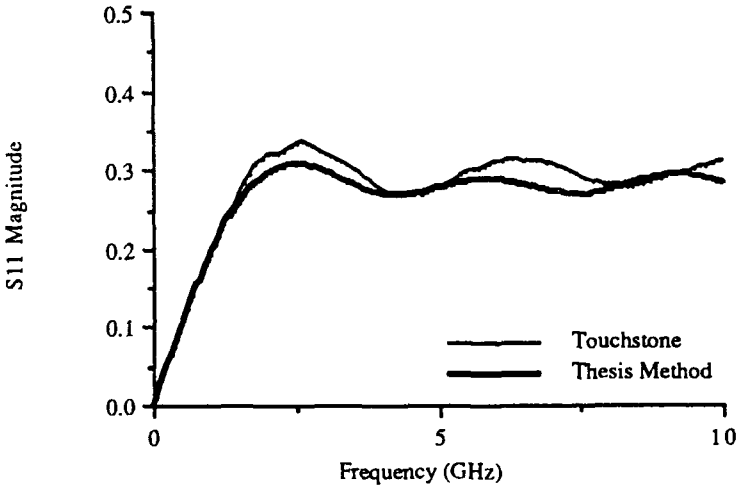

Figure 2.8. Reflection coefficient magnitude comparison between Touchstone and thesis method.

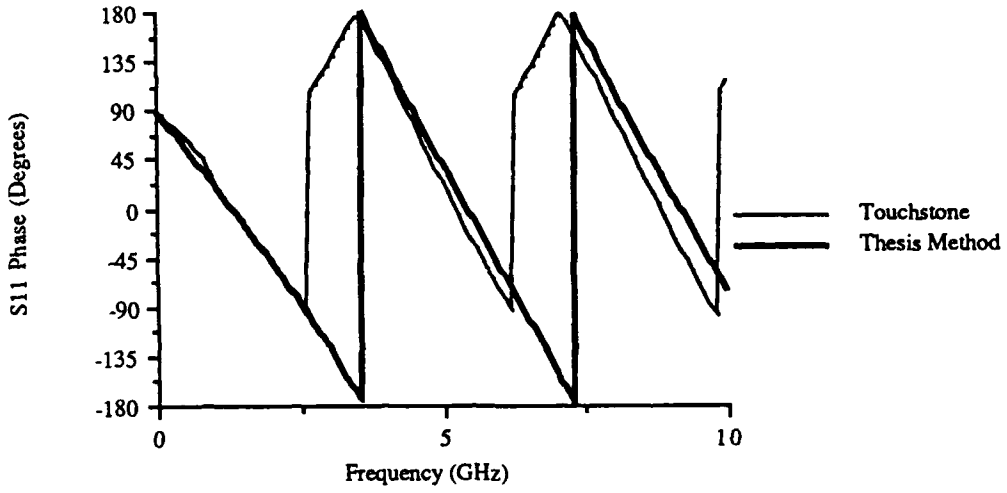

Figure 2.9. Reflection coefficient phase comparison between Touchstone and thesis method.

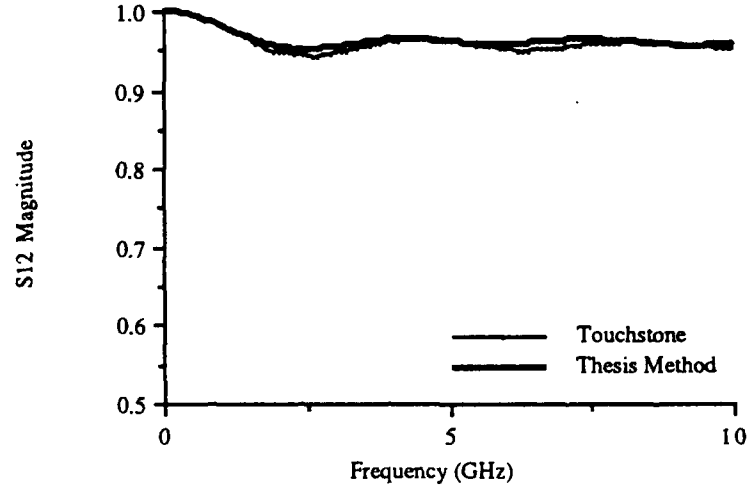

Figure 2.10. Transmission coefficient magnitude comparison between Touchstone and thesis method.

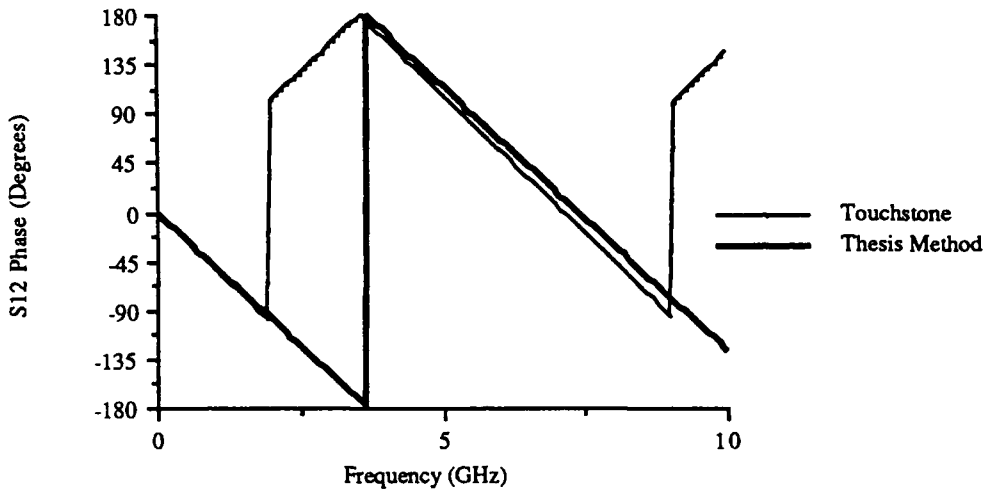

Figure 2.11. Transmission coefficient phase comparison between Touchstone and thesis method.

As an example of the effects of frequency dependence, the overall S-parameters are determined, and the reflection coefficient magnitude is compared to the quasi-static results in Figure 2.12. The curve marked dependent was calculated using the frequency-dependent procedure described in Section 2.2.2, while the curve marked independent came from the quasi-static procedure described in Section 2.2.1. Note that the envelope of the magnitude is about the same, but the nulls are shifted.

2.4. Conclusions

In this chapter, the theory used to characterize a single-line microstrip, both uniform and tapered, was presented. The theory used an integral equation formulation which includes the spatial-domain Green's function. The iteration-perturbation technique required to determine the frequency-dependent characteristics was developed. Once the characteristic impedance Z_0 was determined, the S-parameters for the line were calculated. Results for both uniform and tapered lines were presented. Comparison with previously published results and results from a commercial program showed good agreement. Thus, the technique has been validated for both uniform and tapered single-line microstrips.

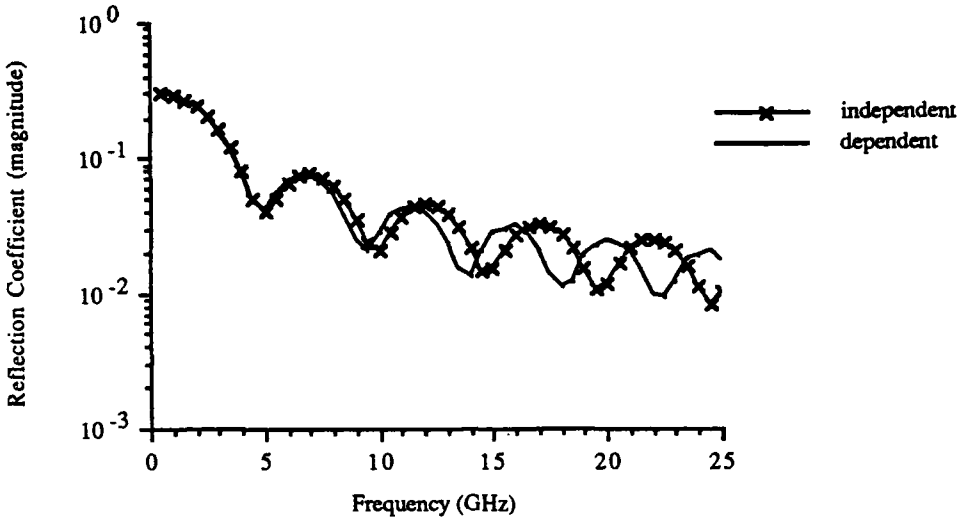

Figure 2.12. Frequency-dependent and quasi-static reflection coefficients for a single-line taper.

CHAPTER 3.

MODELING OF MULTIPLE TAPERED MICROSTRIP LINES

3.1. Introduction

Digital interconnects rarely occur as isolated lines. Many times multiple lines run alongside each other as in a data bus. The proximity of the lines to each other results in coupling between lines and produces a crosstalk signal on the adjacent line. Tapers are typically used as interconnects to change the spacing and width of parallel lines as they approach and connect to an active device, such as an integrated circuit, or a connector, which is found on the edge of a printed circuit board. This chapter takes the model and method developed for a single tapered line and extends it to multiple tapered lines. Only a three-line structure is analyzed in this thesis, but the technique presented could be extended to any number of lines.

Multiple uniform lines have been widely analyzed [3], [8], [16] - [32]. Ghione et al. determined the transfer function of a multiline interconnecting bus using the spectral-domain approach [8]. But while their approach does include losses, it neglects dispersion effects. Diaz [16] used the Discrete Variational Conformal technique which relies on conformal transformations to obtain the simplest possible form of the Green's function. Farr et al. [17] looked specifically at the problem of dispersion and coupling in lines used in very-large-scale integrated circuit (VLSI) interconnections. Garg and Bahl [18] developed semiempirical design equations for two coupled uniform lines. However, none of the previous studies addresses coupled tapered microstrip lines.

This chapter takes the single-line theory presented in Chapter 2 and extends it to multiple tapered lines. Section 3.2 presents the quasi-static and frequency-dependent theory modifications to account for multiple lines. In addition, corrections for thickness and line losses are incorporated. Section 3.3 presents results for both uniform coupled lines and tapered coupled lines. Comparisons are made to previously published results where possible. Finally, conclusions are given in Section 3.4.

3.2. Theory

In this section, the technique developed in Chapter 2 is modified to analyze the three-line tapered microstrip. A cross-sectional view of the three-line taper is shown in Figure 3.1, and a planar view in Figure 3.2. The relative dimensions shown are typical for use in VLSI circuit interconnects, with w being the width-to-height ratio. When referring to a particular line, the numbering scheme in Figure 3.1 is used. When referring to a particular port, as is done by the S-parameters, the numbering scheme in Figure 3.2 is used.

Just as in the single-line case, the three-line taper is solved by first dividing the tapered lines into small sections that can be approximated as uniform coupled lines. The quasi-static **L** and **C** matrices are determined for each uniform section. The frequency-dependent **L** and **C** matrices are found by applying an iteration-perturbation approach based on potential theory. Once the **L** and **C** matrices have been determined, the scattering parameters can be calculated. The inverse Fourier transforms of the scattering parameters are then used in the time-domain simulation.

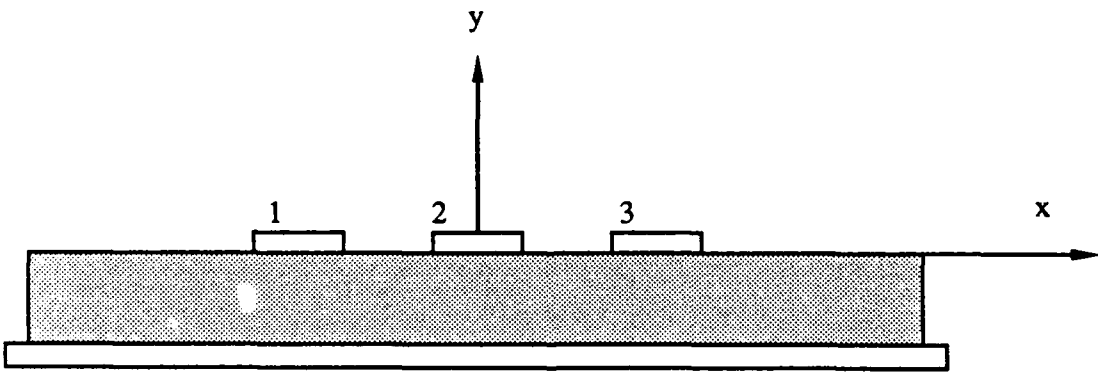

Figure 3.1. Cross sectional view of the three-line taper.

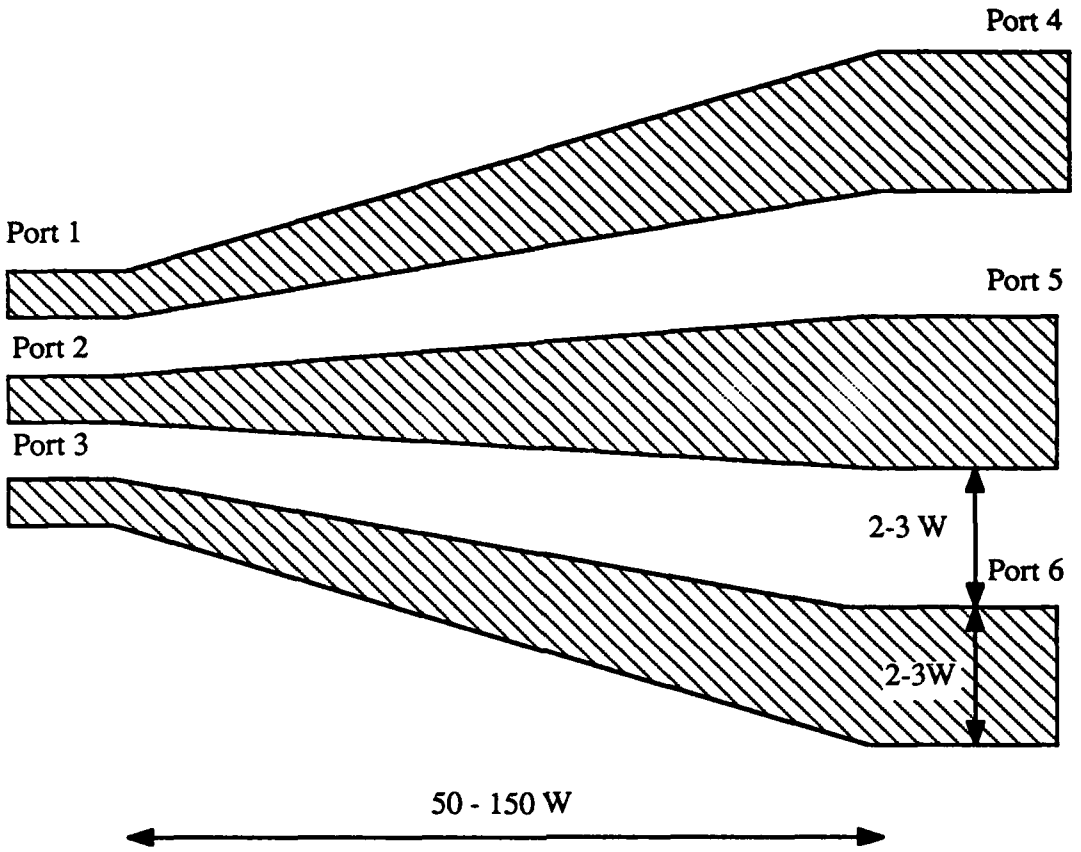

Figure 3.2. Planar view of the three-line taper.

Section 3.2.1 describes the calculation of the quasi-static **L** and **C** matrices. This derivation parallels the one described in Section 2.2.1. Section 3.2.2 presents an overview of the frequency-dependent modifications. Two additional complications are included in the three-line analysis that were not included in the single-line analysis. The first is a correction for finite conductor thickness, and the second is the inclusion of line losses. These complications are covered in Sections 3.2.3 and 3.2.4, respectively. The calculation of scattering parameters is more complicated than for the single-line case, since the structure is now a six-port network. Details are presented in Section 3.2.5.

3.2.1. Quasi-static solution

The procedures of Chapter 2 can be extended to the three-line case. Again, the problem is approached by solving multiple uniform lines and cascading to form multiple tapered lines. The Green's functions now contain both even and odd parts, and the basis functions are replicated on each conductor. This additional complication comes from the fact that three different modes of propagation could exist. Thus, the problem must be solved for three different excitations: two even and one odd. The three independent excitations chosen for the right-hand side are represented by the voltage vectors

$$\mathbf{V} = (V_1, V_2, V_3) = (1,1,1),\ (1,0,1),\ \text{or}\ (-1,0,1). \tag{3.1}$$

Solving the problem gives a 3x3 charge and current matrix, where each element gives the total charge (or total current) for a particular line and mode.

The basic integral equations to be solved are the same as before:

$$\int_{-\infty}^{\infty} G_1^0(x,x')J_z(x')dx' = \frac{A(x)}{\mu_0}, \tag{cf. 2.1}$$

$$\int_{-\infty}^{\infty} G_2^0(x,x')\rho_z(x')dx' = \varepsilon_0\,\phi(x)\ . \tag{cf. 2.2}$$

Now, however, three ranges of x have nonzero values for J_z and ρ_z. These three ranges correspond to the locations of the conductors. Thus, each doubly infinite integral can be reduced to three finite integrals. In addition, symmetry can be imposed to reduce the amount of numerical integration. The even and odd parts of the Green's functions are

$$G_1^0\,(\text{even}) = -\frac{1}{4\pi}\ln|\,x^2 - x'^2\,| + \frac{1}{8\pi}\ln|\,[(2a)^2 + (x+x')^2\,][(2a)^2 + (x-x')^2\,]|, \tag{3.2}$$

$$G_1^0\,(\text{odd}) = -\frac{1}{4\pi}\ln\left(\frac{x+x'}{x-x'}\right) + \frac{1}{8\pi}\ln\left(\frac{(2a)^2 + (x+x')^2}{(2a)^2 + (x-x')^2}\right), \tag{3.3}$$

$$G_2^0\,(\text{even}) = \frac{2}{\kappa_g+1}G_1^0$$

$$+\frac{-\kappa_g}{2\pi(\kappa_g+1)^2}\left(\frac{\kappa_g-1}{2\kappa_g}\ln\frac{\cosh\frac{\pi\alpha}{a}+\cos\frac{\pi\alpha}{2a}(x-x')}{\cosh\frac{\pi\alpha}{a}-\cos\frac{\pi\alpha}{2a}(x-x')}\frac{\cosh\frac{\pi\alpha}{a}+\cos\frac{\pi\alpha}{2a}(x+x')}{\cosh\frac{\pi\alpha}{a}-\cos\frac{\pi\alpha}{2a}(x+x')}\right)$$

$$+\sum_{m=1}^{\infty}(-\eta)^m\ln\frac{\cosh(m+1)\frac{\pi\alpha}{a}+\cos\frac{\pi\alpha}{2a}(x-x')}{\cosh(m+1)\frac{\pi\alpha}{a}-\cos\frac{\pi\alpha}{2a}(x-x')}\frac{\cosh(m+1)\frac{\pi\alpha}{a}+\cos\frac{\pi\alpha}{a}(x+x')}{\cosh(m+1)\frac{\pi\alpha}{a}-\cos\frac{\pi\alpha}{2a}(x+x')},$$

(3.4)

$$G_2^0\,(\text{odd})=\frac{2}{\kappa_g+1}G_1^0$$

$$+\frac{-\kappa_g}{2\pi(\kappa_g+1)^2}\left(\frac{\kappa_g-1}{2\kappa_g}\ln\frac{\cosh\frac{\pi\alpha}{a}-\cos\frac{\pi\alpha}{2a}(x+x')}{\cosh\frac{\pi\alpha}{a}-\cos\frac{\pi\alpha}{2a}(x-x')}\frac{\cosh\frac{\pi\alpha}{a}+\cos\frac{\pi\alpha}{2a}(x+x')}{\cosh\frac{\pi\alpha}{a}+\cos\frac{\pi\alpha}{2a}(x-x')}\right)$$

$$+\sum_{m=1}^{\infty}(-\eta)^m\ln\frac{\cosh(m+1)\frac{\pi\alpha}{a}-\cos\frac{\pi\alpha}{2a}(x+x')}{\cosh(m+1)\frac{\pi\alpha}{a}-\cos\frac{\pi\alpha}{2a}(x-x')}\frac{\cosh(m+1)\frac{\pi\alpha}{a}+\cos\frac{\pi\alpha}{2a}(x+x')}{\cosh(m+1)\frac{\pi\alpha}{a}+\cos\frac{\pi\alpha}{2a}(x-x')}.$$

(3.5)

The total Green's function is the sum of the respective even and odd parts.

For each of the outer conductors, four basis functions are used: two odd and two even. The inner conductor uses two basis functions, either odd or even, depending on the excitation. The two additional odd basis functions are $B_1(x')$ and $B_3(x')$, as defined by Equation (2.4). Analysis showed that two basis functions on the center conductor are sufficient for a symmetric geometry. Expanding $J_z(x')$ and $\rho_z(x')$ in terms of new basis functions and inserting into Equations (2.1) and (2.2), the new equations to be solved are

$$\int_{-\infty}^{\infty}G_1^0(x_i,x')[\sum I_{jm}B_j^*(x')]dx' = \phi_m(x_i)\text{ , and} \qquad (3.6)$$

$$\int_{-\infty}^{\infty} G_2^0(x_i,x')[\sum Q_{jm} B_j^*(x')]dx' = A_m(x_i)\,, \tag{3.7}$$

where the subscript m = 0, 1, 2 designates one of the three modes. For ease of evaluation, a new set of basis functions is defined as follows.

$$B_0^*(x') = B_0(x')\,,\ B_1^*(x') = B_2(x'),\ \text{if even excitation} \tag{3.8}$$

$$B_0^*(x') = B_1(x')\,,\ B_1^*(x') = B_3(x'),\ \text{if odd excitation} \tag{3.9}$$

$$B_k^*(x') = B_{k-2}(x'-s),\ \text{for } k = 2,3,4,5\,. \tag{3.10}$$

For this transformation, s is the center-to-center separation of the microstrip lines, and the lines are normalized so that the width of the center line extends from -1 to 1. Note that $B_0^*(x')$ and $B_1^*(x')$ are nonzero only on the center conductor. Likewise, the other four basis functions are nonzero only on the outer conductors. The derivation from this point onward assumes that the structure is symmetric about the $\hat{y}$-axis, as shown in Figure 3.1, and that all lines have the same width. Such restrictions are not required for the theory, but they do simplify the derivation and subsequent computation significantly.

As before, point matching is used to generate a matrix equation whose solutions are the coefficients I_{jm} and Q_{jm}. The matrix equation must be solved for each excitation. Table 3.1 lists the voltages on each conductor for each mode, as well as the formula for determining the total current on each conductor. The total charge is found by using the Q coefficients instead of the I coefficients. Thus, a 3x3 matrix **I** is formed for the currents and a second 3x3 matrix **Q** is formed for the charges.

From the charge and current matrices, the inductance (**L**) and capacitance (**C**) matrices can be found from $\mathbf{Q} = \mathbf{CV}$ and $\Phi = \mathbf{LI}$. **Q** and **I** have just been determined, and **V** and Φ are given. As a result, **L** and **C** can be determined from

$$\mathbf{L} = \Phi\mathbf{I}^{-1} \text{ and } \mathbf{C} = \mathbf{QV}^{-1}. \tag{3.11}$$

The **L** and **C** values will be used to calculate the S-parameters of the structure in Section 3.2.5.

TABLE 3.1

DEFINITION OF MODES USED TO SOLVE THE THREE-LINE PROBLEM

Mode	Voltages			Current Calculation		
	Line 1	Line 2	Line 3	Line 1	Line 2	Line 3
0	1	1	1	πI_2	πI_0	πI_2
1	1	0	1	πI_2	πI_0	πI_2
2	-1	0	1	$-\pi I_2$	0	πI_2

3.2.2. Frequency-dependent solution

A 1 nsec rise-time pulse has significant Fourier components up to several gigahertz, for which a quasi-static analysis still gives reasonable results. However, as rise times become shorter, a frequency-dependent analysis must be performed. The same technique used to determine the frequency-dependent behavior of a single line can be extended to the three-line structure. Thus, a complete characterization of pulse distortion and crosstalk will be available for a three-line tapered or uniform structure.

The approach used to determine frequency-dependent behavior is similar to that used for a single line. A correction term to the right-hand side of the equation is calculated based on the known $\hat{z}$-directed current in each line and the continuity equation. A new problem arises in that the routine can no longer check for convergence of ε_{eff}, since three different modes now exist. Instead, the routine checks for convergence of total charge and total current.

The basic integral equations to be solved are the same as before:

$$\int_{-\infty}^{\infty} G_1^0(x,x')J_z(x')dx' = \frac{A(x)}{\mu_0} + S(x)\,, \tag{3.12}$$

$$\int_{-\infty}^{\infty} G_2^0(x,x')\rho_z(x')dx' = \varepsilon_0\,\phi(x) + S(x). \qquad (3.13)$$

The correction term S(x) again relates the current and charge through the continuity equation $\nabla_s J = -j\omega\rho$. The correction term is calculated by expanding the charge and current distributions into their Fourier components, and combining the terms with the Green's function as in Equation (2.24). However, this procedure must be done for each conductor. Once the correction term is included in the right-hand side of the matrix equation, solution proceeds as before.

3.2.3. Correction for finite thickness

The quasi-static theory described in the previous section assumes that the conductor is infinitesimally thin. While this assumption may work well for the quasi-static case, it will not work when frequency-dependent parameters and losses must be calculated. One way to account for a finite-thickness conductor is to calculate an effective zero-thickness strip width that takes into account the fringing fields of the finite-thickness conductor. This technique has been frequently used [33] - [35].

The correction terms used here are those proposed by Hammerstad and Jensen [36]:

$$\Delta u_1 = \frac{t}{\pi} \ln\left(1 + \frac{4\exp(1)}{t\coth^2(\sqrt{6.517\,u})}\right) \qquad (3.14)$$

$$\Delta u_r = \frac{1}{2}\left(1 + \frac{1}{\cosh\sqrt{\varepsilon_r - 1}}\right)\Delta u_1\,, \qquad (3.15)$$

where u is the strip width normalized to the substrate height. The corrected strip width u_r is then

$$u_r = u + \Delta u_r\,. \qquad (3.16)$$

This new width-to-height ratio u_r is then used in the calculation of the charge and current distributions. The effect of conductor thickness on the width-to-height ratio is shown in Figure 3.3. The correction is smaller for higher values of the relative dielectric constant. This is consistent with the fact that more of the field is concentrated in the substrate because of the higher dielectric constant; thus, the fringing field is relatively smaller.

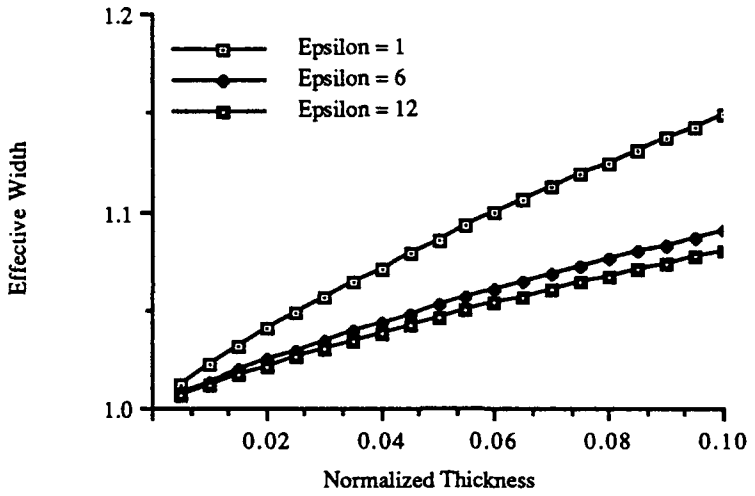

Figure 3.3. Effective width-to-height ratio for nominal width-to-height ratio of 1 when thickness of conductor is considered.

3.2.4. Line losses

An important concern for computer-aided design is the inclusion of line losses. Large losses can be encountered in thin or narrow lines, causing the attenuation of the pulse as it propagates. Fortunately, losses can be included in the calculation of the impedance (**Z**) and admittance (**Y**) matrices. Specifically,

$$\mathrm{Re}\{\mathbf{Z}\} = \mathbf{R}\,, \tag{3.17}$$

$$\mathrm{Im}\{\mathbf{Z}\} = \omega\mathbf{L}\,, \tag{3.18}$$

and

$$\mathrm{Re}\{\mathbf{Y}\} = \mathbf{G}\,, \tag{3.19}$$

$$\mathrm{Im}\{\mathbf{Y}\} = \omega\mathbf{C} \tag{3.20}$$

where **R** is the resistivity in ohms per meter and **G** is the conductivity between lines in mhos per meter. The conductance matrix is related to the dielectric losses. If the dielectric losses are small, then **G** can be ignored [8]. Then, the **ZY** and **YZ** matrices are formed, and the complex eigenvalues and eigenvectors can be found as described in Section 3.2.5.

The propagation constants γ_i are determined from the $\gamma_i^2 = i^{th}$ eigenvalue of **YZ**, which will have a real part if the lines are lossy. Thus, the factor $\Psi_{ii} = e^{-\gamma_i z}$ will have a real part which will cause the attenuation of the pulse. For a lossless line, γ_i will be purely imaginary, and no attenuation will occur.

The problem, however, is how to determine the **R** matrix. This thesis assumes that the dielectric losses are small so that they can be neglected, or that if the dielectric losses are not small, then they are given. The quasi-static theory described previously will produce the **L** and **C** matrices. The **R** matrix can be calculated using the geometry of the microstrip interconnect and the conductivity of the lines. The basic principle is [37]:

$$R_i = \frac{l_i}{\sigma_i S_i}, \tag{3.21}$$

where l_i is the length of the conductor, σ_i is the conductivity, and S_i is the cross-sectional area. R_i here is just the value of resistance for one particular line. Letting l_i equal 1 meter gives the resistance on a per meter basis,

$$R_i = \frac{1}{\sigma_i S_i} \ \Omega/m, \tag{3.22}$$

provided σ_i and S_i have dimensional units in terms of meters.

Frequency dependence comes in through the determination of the cross-sectional area S_i. Figure 3.4 shows a single microstrip conductor with a skin depth δ indicated. The value of δ is given by

$$\delta = \sqrt{\frac{2}{\omega \mu_0 \sigma}}. \tag{3.23}$$

If δ is greater than $\frac{t}{2}$, then the cross-sectional area is given by the quasi-static value for the entire structure:

$$S_i = Wt. \tag{3.24}$$

However, as the frequency increases, the skin depth decreases. The conductor can be treated as if all the current were contained within one skin depth of the surface [37, p. 388]. Thus, the cross-sectional area is frequency dependent, and is given by

$$S_i = 2\,\delta\,(t + W - 2\,\delta) \tag{3.25}$$

whenever the skin depth becomes less than $\frac{t}{2}$.

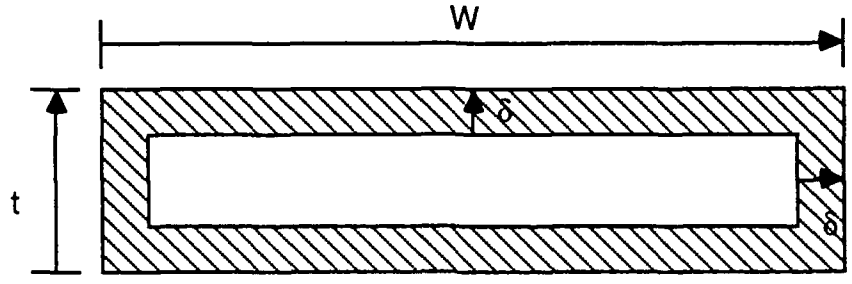

Figure 3.4. *Geometry for calculation of cross-sectional area due to skin depth.*

The **R** matrix is then given by

$$\mathbf{R} = \begin{bmatrix} R_1 & 0 & 0 \\ 0 & R_2 & 0 \\ 0 & 0 & R_3 \end{bmatrix}, \tag{3.26}$$

where typically $R_1 = R_2 = R_3$. The off-diagonal terms are typically zero since no connection exists between the lines, and the frequencies are below those of millimeter waves [8]. Thus, the effect of line losses can easily be evaluated by including them as the real part of the impedance matrix **Z**.

An alternative method of handling conductor losses is based on Wheeler's incremental inductance rule [10], [38]. This method is based on the fact that for a conductor with surface impedance $Z_s = R + jX$,

$$R = X = \omega L_i \,, \tag{3.27}$$

where L_i is the incremental increase in L caused by an incremental recession of all metallic walls due to the skin effect. This technique has been applied to single conductor lines [34], [39], but no application has been made to multiple lines, perhaps because the expression for L_i is difficult to compute analytically for multiconductor lines. The expression is

$$L_i = \frac{\delta}{2} \sum_m \frac{\delta L}{\delta n_m} \tag{3.28}$$

where m is the m^{th} conductor wall and $\frac{\delta L}{\delta n_m}$ is the derivative of L with respect to the recession of wall m. Of more interest here is the expression for the resistance:

$$R = \frac{R_{sm}}{\mu_0} \sum_m \frac{\delta L}{\delta n_m}, \tag{3.29}$$

where $R_{sm} = \frac{\omega \mu_m \delta_m}{2}$ and $\delta_m = \sqrt{\frac{2}{\omega \mu_m \sigma_m}}$ as before. For the case under consideration here, $\mu_m = \mu_0$ and $\sigma_m = \sigma$.

The difficulty in using Wheeler's incremental inductance rule comes in computing $\frac{\delta L}{\delta n_m}$. As with any numerical method, the approximation

$$\frac{\Delta L}{\Delta n_m} \approx \frac{\delta L}{\delta n_m} \tag{3.30}$$

must be used. This method was compared to the simple skin effect resistance calculation discussed previously. The difference between the scattering parameters was found to be negligible (less than 0.1%). The comparison was made from quasi-static up to 6 GHz. However, Wheeler's incremental inductance rule has the disadvantage that it requires the **L** matrix to be calculated four times in addition to the one time required for the baseline calculation of **L**. The simple skin effect formula requires only the baseline calculation, which would have to be done even if the conductors were assumed lossless. Thus, the data shown in this thesis use the simple skin effect calculation for the sake of numerical efficiency.

3.2.5. Scattering parameter determination

The procedure for finding the S parameters is more complicated in the three-line case. Again, the problem is first solved for small sections of a uniform three-line structure. However, three different propagating modes exist, with each mode possessing a different propagation constant. The problem is best worked using modal parameters, converting to line parameters only when needed. The modal eigenvectors are the eigenvectors of the **ZY** (or **YZ**) matrix. These eigenvalues are proportional to the modal propagation constants, and are used to form a similarity transformation between line and modal variables. Thus, the original problem is converted to a modal problem.

First, the eigenvalues and eigenvectors of the **ZY** and **YZ** matrices are determined. The inverse of the matrix of column vectors of **YZ** is called **H**, and the inverse of the matrix of column vectors of **ZY** is called **E**. The $\mathbf{QI}^{-1}$ is analogous to **YZ**, but the $\mathbf{I}^{-1}\mathbf{Q}$ matrix must be premultiplied by Φ^{-1} and post-multiplied by **V**. The **E** and **H** matrices are then normalized so that the first element of each row equals one. The eigenvalues, which are the same for either $\mathbf{QI}^{-1}$ or $\Phi\mathbf{I}^{-1}\mathbf{QV}^{-1}$, are placed in the diagonal of the matrix Λ_{ref}. The reference impedance matrix is calculated from $\mathbf{Z}_{ref} = \Lambda_{ref}^{-1}\mathbf{E}_{ref}\Phi\mathbf{I}^{-1}\mathbf{H}_{ref}^{-1}$. The matrix $\mathbf{Z}_{ref}$ is the matrix containing the modal impedances. With the reference calculations done, we obtain the impedance matrix of the test section by the same procedure.

The modal reflection coefficient is given by $\Gamma = [\mathbf{1}+\mathbf{FW}]^{-1}[\mathbf{1}-\mathbf{FW}]$, where $\mathbf{F} = \mathbf{E}\mathbf{E}_{ref}^{-1}$ and $\mathbf{W} = \mathbf{Z}_{ref}\mathbf{H}_{ref}\mathbf{H}^{-1}\mathbf{Z}^{-1}$. The propagation matrix is

$$\Psi = \begin{pmatrix} e^{-\gamma_1 l} & 0 & 0 \\ 0 & e^{-\gamma_2 l} & 0 \\ 0 & 0 & e^{-\gamma_3 l} \end{pmatrix}, \tag{3.31}$$

where γ_i is the propagation constant for that mode and l is the length of the section. We also need $\mathbf{T} = [\mathbf{1}+\mathbf{FW}]^{-1}\mathbf{F}$. The S parameters are then given by

$$\mathbf{S}_{11} = \mathbf{T}^{-1}\,[\Gamma - \Psi\Gamma\Psi]\,[\mathbf{1} - \Gamma\Psi\Gamma\Psi]^{-1}\,\mathbf{T} \tag{3.32}$$

$$\mathbf{S}_{22} = \mathbf{S}_{11} \tag{3.33}$$

$$\mathbf{S}_{21} = 2\mathbf{E}_0\mathbf{E}^{-1}\,[\mathbf{1} - \Gamma]\,\Psi\,[\mathbf{1} - \Gamma\Psi\Gamma\Psi]^{-1}\,\mathbf{T} \tag{3.34}$$

$$\mathbf{S}_{12} = \mathbf{S}_{21}, \tag{3.35}$$

where Γ is the modal reflection matrix, Ψ is the modal propagation matrix, $\mathbf{E}$ and $\mathbf{E}_0$ are the eigenvector matrices, and $\mathbf{T}$ is the transformation matrix. The technique used here is based on work done by Schutt-Aine [40]. The uniform sections are cascaded using the following equations:

$$\mathbf{S}_{11}^{comp} = \mathbf{S}_{11}^{1} + \mathbf{S}_{12}^{1}\mathbf{S}_{11}^{2}[\mathbf{1} - \mathbf{S}_{22}^{1}\mathbf{S}_{11}^{2}]^{-1}\,\mathbf{S}_{21}^{1} \ , \tag{3.36}$$

$$\mathbf{S}_{21}^{comp} = \mathbf{S}_{21}^{2}[\mathbf{1} - \mathbf{S}_{22}^{1}\mathbf{S}_{11}^{2}]^{-1}\,\mathbf{S}_{21}^{1} \ , \tag{3.37}$$

$$\mathbf{S}_{22}^{comp} = \mathbf{S}_{22}^{2} + \mathbf{S}_{21}^{2}\mathbf{S}_{22}^{1}[\mathbf{1} - \mathbf{S}_{11}^{2}\mathbf{S}_{22}^{1}]^{-1}\,\mathbf{S}_{12}^{2} \ , \text{ and} \tag{3.38}$$

$$\mathbf{S}_{12}^{comp} = \mathbf{S}_{12}^{1}[\mathbf{1} - \mathbf{S}_{11}^{2}\mathbf{S}_{22}^{1}]^{-1}\,\mathbf{S}_{12}^{2} \ . \tag{3.39}$$

The superscript comp indicates the composite matrix, while the superscripts 1 and 2 indicate the first and second set of S-parameter matrices.

3.3. Results

The techniques described in Section 3.2 were implemented in a computer program. In this section, results for particular uniform line and tapered line test cases are presented. Comparisons are made to published results where possible.

3.3.1. Uniform line results

As previously stated, the S-parameters for the tapered structure are obtained by cascading small uniform sections of a three-line structure. As a check of uniform line results, a test example was run using the parameters listed in Table 3.2. Some S-parameter results for three-line uniform structures are shown in Figures 3.5 through 3.8. Figures 3.6 and 3.8 show that the coupling between lines increases as the frequency increases. Recall that the subscripts for the S-parameters follow the convention shown in Figure 3.2.

3.3.2. Tapered line results

As done for the single-line case, the S-parameters for the tapered three-line structure are obtained by cascading small uniform three-line sections. A test example was run using the parameters listed in Table 3.3. Some S-parameter results for a three-line tapered structure are shown in Figures 3.9 through 3.12. Notice that the shape of the reflection coefficient shown in Figure 3.9 is more complicated than the corresponding result for

uniform lines shown in Figure 3.5. Also, Figures 3.10 and 3.12 indicate that coupling increases with frequency, just as for coupled uniform lines.

TABLE 3.2

PARAMETERS FOR UNIFORM LINE TEST CASE

Length of line	78.74 mm
Width of line	0.7874 mm
Spacing of line	0.7874 mm
Conductor thickness	0.03556 mm
Conductivity (copper)	5.8×10^7 mhos/m
Dielectric thickness	0.7874 mm
Relative dielectric constant	4.7

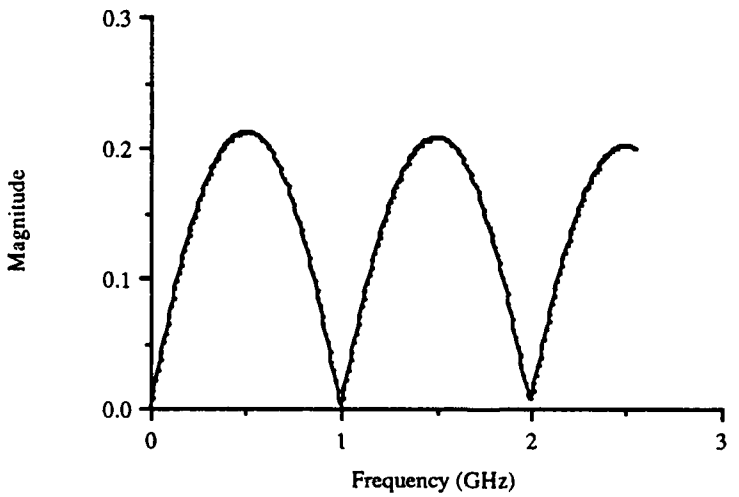

Figure 3.5. S_{22} for a uniform three-line structure.

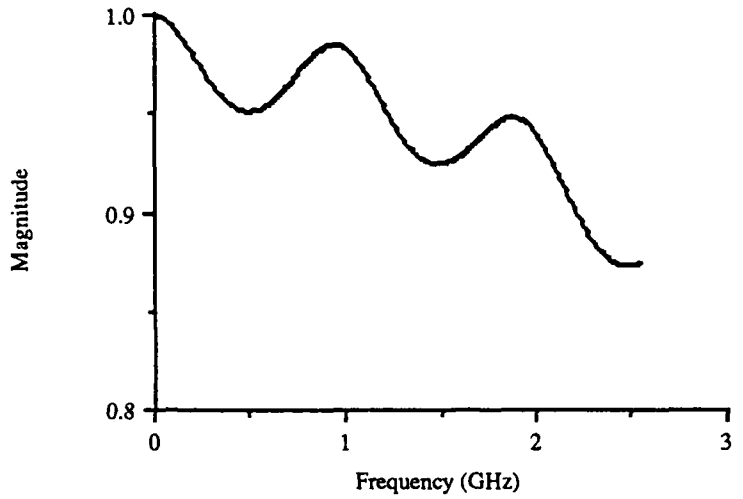

Figure 3.6. S_{25} for a uniform three-line structure.

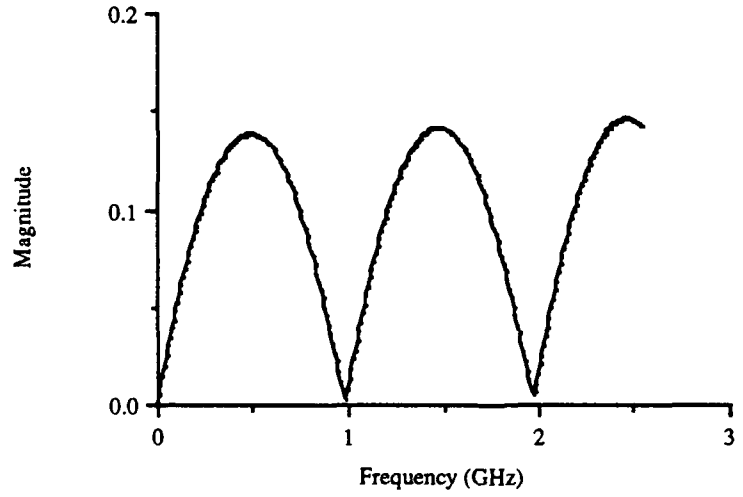

Figure 3.7. S_{12} for a uniform three-line structure.

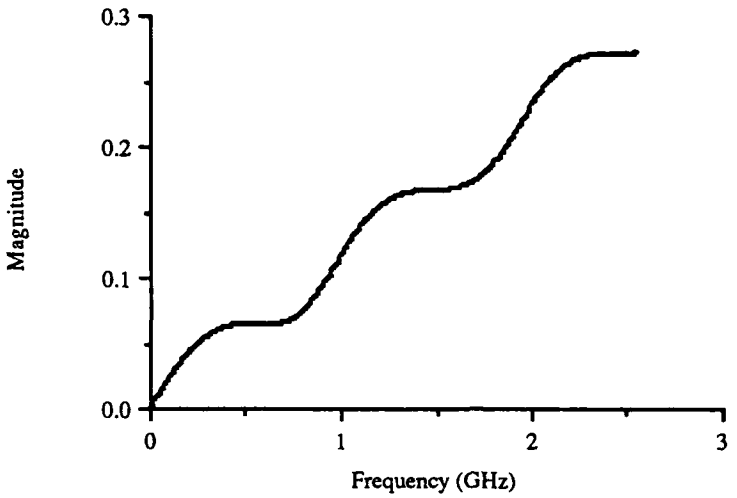

Figure 3.8. S_{15} for a uniform three-line structure.

TABLE 3.3	
PARAMETERS FOR TAPERED LINE TEST CASE	
Length of line	78.74 mm
Width of line (input end)	0.7874 mm
Width of line (output end)	1.9685 mm
Spacing of line (input end)	0.7874 mm
Spacing of line (output end)	1.9685 mm
Conductor thickness	0.03556 mm
Conductivity (copper)	5.8×10^7 mhos/m
Dielectric thickness	0.7874 mm
Relative dielectric constant	4.7

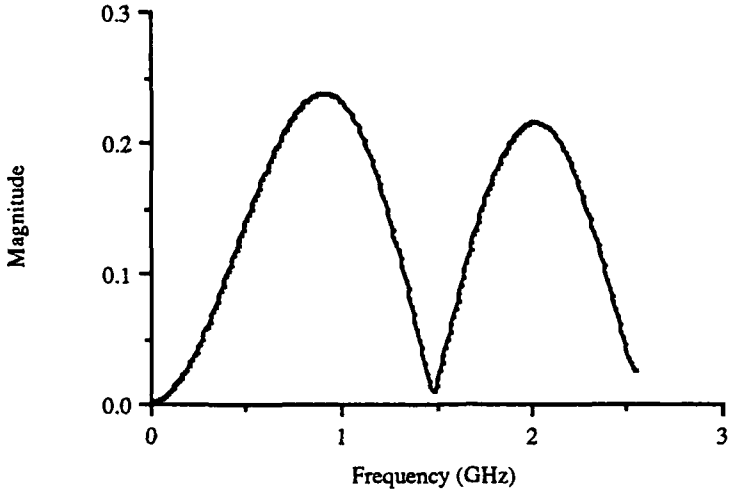

Figure 3.9. S_{22} for a tapered three-line structure.

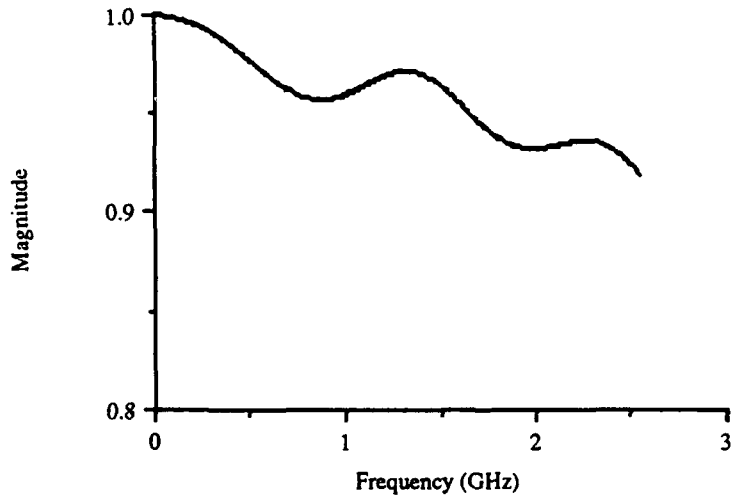

Figure 3.10. S_{25} for a tapered three-line structure.

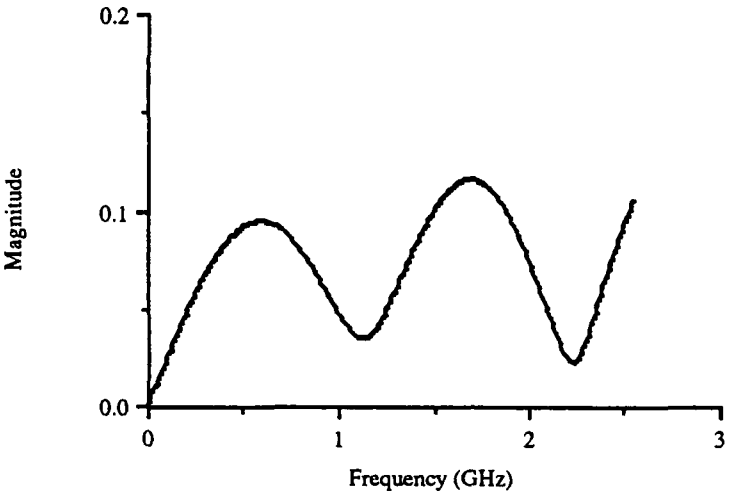

Figure 3.11. S_{12} for a tapered three-line structure.

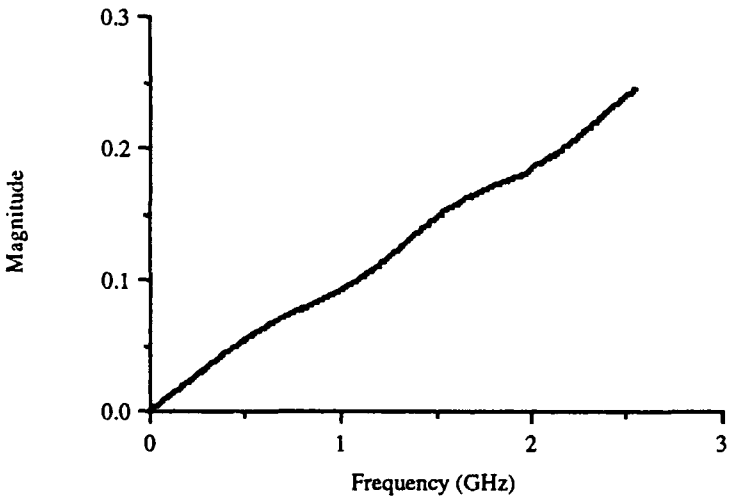

Figure 3.12. S_{15} for a tapered three-line structure.

3.4. Conclusions

In this chapter, the technique developed for a single-line taper was extended to a three-line tapered structure. For this case, the problem had to be solved for three different excitations in order to account for the three different propagating modes. The result was a matrix of charge and current values. The effects of conductor thickness and losses were included. The method for determining the scattering parameters was presented. Results were shown for a typical uniform and tapered three-line structure.

CHAPTER 4.

TIME-DOMAIN SIMULATION OF MULTIPLE TAPERED MICROSTRIP LINES

4.1. Introduction

An important concern of this study is the effect that tapered lines have on high-speed digital data pulses. These pulses can have a rise time of less than 1 nanosecond (nsec). The results are desired not only for linear terminations, but also for nonlinear terminations. The study of linear terminations is undertaken in this thesis for two reasons. First, this is the simplest case, and the results in many instances are intuitive and easily verified. Second, much work has already been done and published using linear terminations; thus, many results are available for comparison. Nonlinear terminations must be included because the inputs of active devices are typically modeled with nonlinear elements. The solution of such a problem cannot be accomplished in the frequency domain, because nonlinear elements cannot be modeled in the frequency domain. Thus, a time-domain simulation is required. This chapter describes how that time-domain simulation is performed.

Within the last few years, several articles have been published on the time-domain analysis of transmission lines [8], [9], [13], [40] - [42]. Goossen and Hammond were concerned with a single microstrip line on a silicon substrate [13]. They used empirical equations for dispersion and loss, and a transform technique for the linear terminations. The technique used by Romeo and Santomauro [9] is similar to the one used in this thesis and [40] in that they convert the coupled lines into modal parameters propagating on uncoupled uniform lines. Models for nonlinear devices have been developed for use in circuit simulators and are readily available [43]. However, the use of these models as terminations for microstrip transmission lines is relatively new. Schutt-Aine [40] analyzed coupled uniform microstrip lines with typical digital drivers and receivers modeled as nonlinear devices. Hill and Mathews analyzed pulse propagation on an exponential transmission line with nonlinear drivers and receivers [42], but their method is limited to exponential lines, which rarely occur in digital systems.

In this chapter, the necessary theory is presented to analyze the effect of coupled, tapered microstrip lines on digital pulses. Section 4.2 describes the termination modeling

and algorithm for calculating the time-domain response. Equations are developed which can be implemented on a digital computer. Section 4.3 presents the results of the time-domain simulation for a typical coupled, tapered microstrip structure. These results show the effect of the nonlinear terminations and of the coupling between lines. Finally, Section 4.4 contains the summary and conclusions.

4.2. Theory

The voltage response of a tapered microstrip line to an input pulse is found by time-domain simulation. The time-domain simulation is performed by convolving the input voltage vector with the time-domain Green's function matrix corresponding to the S-parameters. The S-parameters are those derived using the method presented in Chapter 3. The time-domain Green's function matrix is the inverse Fourier transform of the frequency-domain S-parameters. The simulation incorporates the effects of the terminations through the reflection and transmission coefficient matrices calculated from the source and load impedances. If the termination is nonlinear, a Newton-Raphson algorithm is used to incorporate the V-I characteristics of the termination at the corresponding time step. Thus, the problem can be reduced to one of solving a linear transmission line problem for the given time step and given iteration on the nonlinear termination. Once the solution converges for the given time step, the process is repeated for the next time step, using the previous results as a starting point.

In Chapter 3, a method of determining the frequency-domain scattering parameters was developed. These scattering parameters satisfy the relationships

$$\mathbf{B}_1 = \mathbf{S}_{11}\,\mathbf{A}_1 + \mathbf{S}_{12}\,\mathbf{A}_2\,, \tag{4.1}$$

$$\mathbf{B}_2 = \mathbf{S}_{21}\,\mathbf{A}_1 + \mathbf{S}_{22}\,\mathbf{A}_2\,, \tag{4.2}$$

where $\mathbf{S}_{11}$, $\mathbf{S}_{12}$, $\mathbf{S}_{21}$, and $\mathbf{S}_{22}$ are the modal scattering parameter matrices determined in Chapter 3 that describe the six-port network. $\mathbf{A}_1$, $\mathbf{A}_2$, $\mathbf{B}_1$, and $\mathbf{B}_2$ are the forward and backward modal wave matrices. For the six-port network, the subscript 1 indicates the input ports (ports 1, 2, and 3), while the subscript 2 indicates the output ports (ports 4, 5, and 6). A time-domain formulation can be achieved by taking an inverse Fourier transform of (4.1) and (4.2) to obtain

$$\mathbf{b}_1(t) = \mathbf{S}_{11}(t) * \mathbf{a}_1(t) + \mathbf{S}_{12}(t) * \mathbf{a}_2(t)\,, \tag{4.3}$$

$$\mathbf{b}_2(t) = \mathbf{S}_{21}(t) * \mathbf{a}_1(t) + \mathbf{S}_{22}(t) * \mathbf{a}_2(t) , \tag{4.4}$$

where each term is the inverse Fourier transform of the corresponding term in (4.1) or (4.2), and the symbol * denotes convolution.

Equations (4.3) and (4.4) relate the incident and reflected time-domain wave vectors. The wave vectors are related to the terminations and the input signals by the equations

$$\mathbf{a}_1(t) = \mathbf{T}_1(t)\, \mathbf{g}_1(t) + \Gamma_1(t)\, \mathbf{b}_1(t) , \tag{4.5}$$

$$\mathbf{a}_2(t) = \mathbf{T}_2(t)\, \mathbf{g}_2(t) + \Gamma_2(t)\, \mathbf{b}_2(t) , \tag{4.6}$$

where $\mathbf{T}_1(t)$ and $\mathbf{T}_2(t)$ are the transmission coefficient matrices, $\Gamma_1(t)$ and $\Gamma_2(t)$ are the reflection coefficient matrices, and $\mathbf{g}_1(t)$ and $\mathbf{g}_2(t)$ are the voltage generator vectors.

Thus, Equations (4.3) through (4.6) relate the source voltages, terminations, and characteristics of the transmission line structure. These can then be solved for $\mathbf{a}_1(t)$, $\mathbf{a}_2(t)$, $\mathbf{b}_1(t)$, and $\mathbf{b}_2(t)$. The modal voltage vectors are then given by

$$\mathbf{V}_{m1}(t) = \mathbf{a}_1(t) + \mathbf{b}_1(t) \tag{4.7}$$

$$\mathbf{V}_{m2}(t) = \mathbf{a}_2(t) + \mathbf{b}_2(t) . \tag{4.8}$$

The line voltage vectors are recovered from

$$\mathbf{V}_1(t) = \mathbf{E}_0^{-1}\, \mathbf{V}_{m1}(t) \tag{4.9}$$

$$\mathbf{V}_2(t) = \mathbf{E}_0^{-1}\, \mathbf{V}_{m2}(t) , \tag{4.10}$$

where $\mathbf{E}_0$ is the voltage eigenvector matrix.

The input and output terminations can be characterized by their reflection and transmission coefficient matrices. The matrices are defined by [40]

$$\Gamma_s(t) = -\, [\mathbf{I} + \mathbf{E}\, \mathbf{Z}_s(t)\, \mathbf{L}^{-1}\, \mathbf{E}^{-1}\, \Lambda_m]^{-1}\, [\mathbf{I}_n - \mathbf{E}\, \mathbf{Z}_s(t)\, \mathbf{L}^{-1}\, \mathbf{E}^{-1}\, \Lambda_m]^{-1} , \tag{4.11}$$

$$\Gamma_l(t) = [\mathbf{I} + \mathbf{E}\, \mathbf{Z}_l(t)\, \mathbf{L}^{-1}\, \mathbf{E}^{-1}\, \Lambda_m]^{-1}\, [\mathbf{I}_n - \mathbf{E}\, \mathbf{Z}_l(t)\, \mathbf{L}^{-1}\, \mathbf{E}^{-1}\, \Lambda_m]^{-1} , \tag{4.12}$$

$$\mathbf{T}_s(t) = [\mathbf{I} + \mathbf{E}\, \mathbf{Z}_s(t)\, \mathbf{L}^{-1}\, \mathbf{E}^{-1}\, \Lambda_m]^{-1} , \tag{4.13}$$

$$\mathbf{T}_l(t) = [\mathbf{I} + \mathbf{E}\,\mathbf{Z}_l(t)\,\mathbf{L}^{-1}\,\mathbf{E}^{-1}\,\Lambda_m]^{-1}\,, \tag{4.14}$$

where **I** is the identity matrix, the subscript s or l denotes the source or load end of the structure, and **E**, **L**, and Λ are calculated from the reference system.

A typical load for a transmission line includes digital receivers that contain nonlinearities. In addition, capacitance can be introduced by the chip bonding pad, package, and printed wiring board connector [44, p. 39]. These effects must be included in a time-domain simulation if accurate results are desired. In order to determine the impedance matrices for nonlinear loads, the V-I (i. e., voltage-current) characteristics are used in a Newton-Raphson algorithm to calculate the impedance at that time step. To perform a Newton-Raphson iteration, the nonlinear equation for the voltage-current relationship is put in the form $f(x) = 0$ and the algorithm

$$x^{(j+1)} = x^{(j)} - \left[\frac{df(x)}{dx}\Big|_{x = x^{(j)}}\right]^{-1} f(x^{(j)}) \tag{4.15}$$

is applied. If the initial guess $x^{(0)}$ is sufficiently close to a correct solution of $f(x) = 0$, then the algorithm will always converge to a correct solution. If the initial guess is far away from a correct solution, the algorithm may not converge at all. For the problem under consideration, the initial guess $x^{(0)}$ at a time step is chosen to be the final value from the previous time step. Thus, the initial guess is assured of being close to a correct solution, and the algorithm will converge. Convergence to a solution is quadratic.

Once the voltage and current values are found, the impedances are determined, and the solution proceeds as in the linear case. This technique was implemented in a computer program, with the results shown in Section 4.3.

4.3. Results

The time-domain theory presented in this chapter was combined with the tapered line model developed in Chapter 3. This combination allows the input and output voltage waveforms of a six-port, three-line tapered structure to be determined. First, comparisons are made with previously published uniform line results. Then, a test case is run using the geometry analyzed in Chapter 3. Results for both linear and nonlinear terminations are presented.

Unfortunately, no time-domain results are available for tapered lines. Therefore, to verify the technique, a comparison was made with the time-domain results of Romeo and

Santomauro [9]. Even though they analyzed a uniform line, a comparison of results would confirm the time-domain simulation technique. The parameters used in [9] are listed in Table 4.1. The results are shown in Figure 4.1. As can be seen, agreement is good, considering that the data from [9] were read from a graph published in the article.

TABLE 4.1

PARAMETERS FOR COMPARISON WITH ROMEO AND SANTOMAURO

Line width	0.19 mm
Line spacing	0.44 mm
Conductor thickness	0.06 mm
Height of substrate	0.41 mm
Length of line	210.0 mm
Relative dielectric constant	4.6
Pulse rise time	5.0 nsec

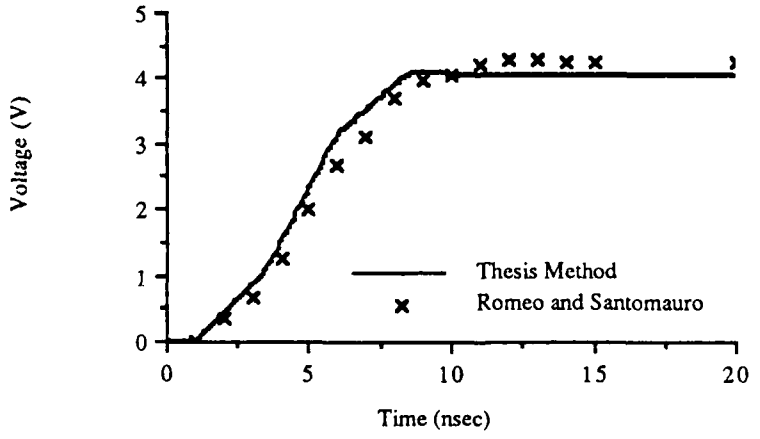

Figure 4.1. Comparison of thesis method with the results of Romeo and Santomauro [9].

The test case to be considered is a set of coupled, tapered microstrip lines using the parameters listed in Table 4.2. The geometry of the tapered structure is the same as used in Chapter 3 and listed in Table 3.3. An input pulse of 4 V was placed on the center line, and the voltages at the input and output ends of all three lines were calculated.

TABLE 4.2

PARAMETERS FOR TIME-DOMAIN SIMULATION

Rise and fall time	0.5 nsec
Pulse width	10 nsec
Source voltage (ports 1, 2, 3)	0, 4, 0 V
Loads	Nonlinear
Duration of simulation	20 nsec
Number of data points	256

Figures 4.2 through 4.5 show the time-domain response of a three-line structure with nonlinear loads. In Figure 4.2, the reflection from the load is evident by the step in the rise and fall times. The fact that the voltage levels are not constant across these steps is due to the nonlinearities of the terminations. The effect of the terminations can also be seen in Figure 4.4. Figures 4.3 and 4.5 show that the crosstalk signal has an amplitude of about 200 mV. Thus, any devices connected to the coupled transmission lines must have a noise margin large enough to prevent the crosstalk signal from causing false switching. The dependence of the crosstalk signal on the transmission line geometry can easily be determined by evaluating other cases.

4.4. Conclusions

In this chapter, the equations for the time-domain simulation were presented. These equations take the frequency-domain scattering parameters developed in Chapter 3 and combine them with the nonlinear terminations to obtain the voltage waveforms for all six ports. This allows the study of pulse propagation through the tapered line and crosstalk between tapered lines. Results were presented for a typical example. Agreement with previously published results was shown to be good.

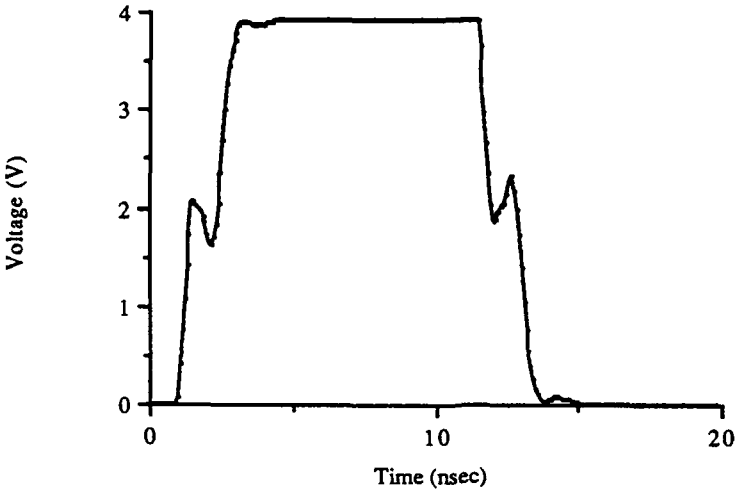

Figure 4.2. Voltage at input of center line of three-line taper.

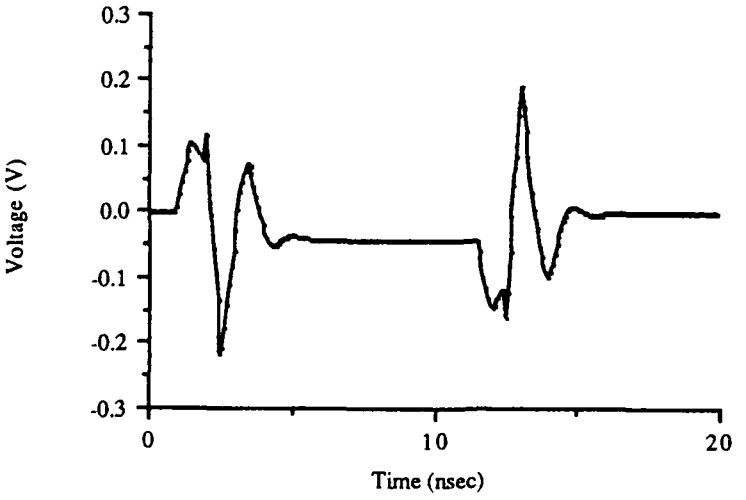

Figure 4.3. Voltage at input of outer line of three-line taper.

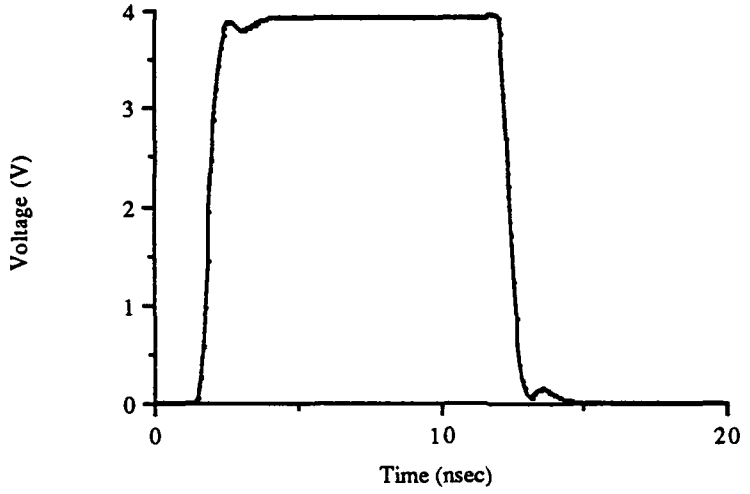

Figure 4.4. Voltage at output of center line of three-line taper.

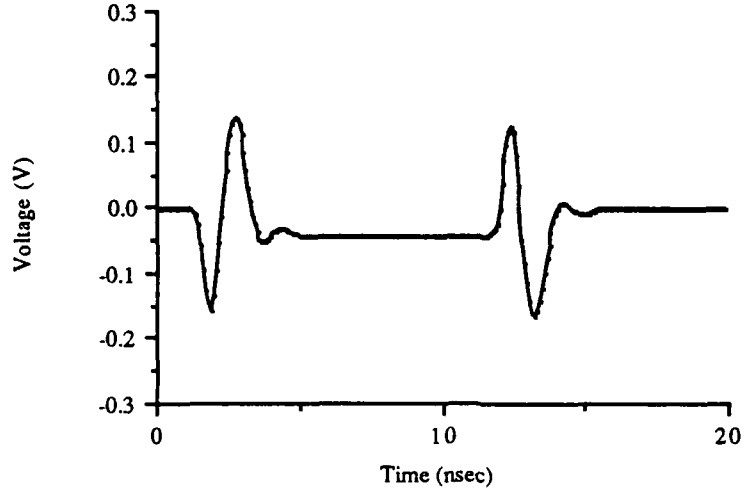

Figure 4.5. Voltage at output of outer line of three-line taper.

CHAPTER 5.

EXPERIMENTAL CHARACTERIZATION OF MULTIPLE TAPERED MICROSTRIP LINES

5.1. Introduction

The S-parameters computed using the approach described in Chapters 2 and 3 will be compared to measurements taken on representative structures. In particular, a single uniform line and a three-line tapered structure will be measured. These measurements will confirm the validity of the model and the accuracy of the computer program. Possible measurement errors will be discussed.

Several authors have reported experimental S-parameter results for uniform microstrip lines [6], [8], [40]. For example, Schutt-Aine [40] performed experimental time-domain measurements on coupled uniform lines. But only one of these papers concerned itself with tapered microstrip lines. Syahkal and Davies [6] performed measurements on back-to-back microstrip to coplanar waveguide tapers and a tapered finline to waveguide transition. Unfortunately, neither of these structures is of interest in high-speed digital circuits.

In this chapter, experimental measurements are compared to the calculated values. Section 5.2 describes the procedures used to obtain the experimental data. The data consist of both magnitude and phase values for each S-parameter. Section 5.3 shows the experimental data as well as the data calculated by the program. Finally, Section 5.4 presents the conclusions drawn from the comparison of the experimental measurements with the calculated results.

5.2. Test Procedures

The tests were made using a Hewlett-Packard HP8510B network analyzer, which provides the reflection and transmission coefficients of the structure. These values are then compared with the calculated values. Measurements were made on a single-line and a three-line geometry. Table 5.1 lists the parameters of the single-line test case. All complex S-parameters (S_{11}, S_{12}, S_{21}, and S_{22}) were measured.

TABLE 5.1	
PARAMETERS FOR UNIFORM LINE TEST CASE	
Line length	10.16 cm
Line width	1.397 mm
Substrate thickness	0.7874 mm
Relative dielectric constant	4.7
Conductor conductivity (copper)	5.8×10^7 mhos/m
Conductor thickness	0.03556 mm
Additional length from connectors	1.0 cm

The first step in taking the measurements was to calibrate the HP8510B. The calibration was done using specially-fabricated shorts, opens, matched loads, and sliding loads on both ports. The calibration was then checked by observing the S-parameters of a through-section and an open. The results were as expected. A TRL (through-reflected line) calibration was tried to remove the effect of the connectors, but could not be successfully accomplished due to the lack of a lossless reference line. Therefore, all measurements include the effects of the connectors. Symmetry was used to reduce the number of measurements taken. The results of the measurements are presented in the next section, where they are compared with the calculated S-parameters.

5.3. Results

This section presents the results of the experimental measurements and compares them with the results of the calculations. Due to the connectors in the lines, the data from the experimental measurements are valid only to about 4 GHz. Thus, the comparisons to calculated results will be made only up to 4 GHz. The length introduced by the connectors is already in the experimental results, and therefore was included in the calculated results. Additionally, the board used for measurements had a film layer over the conductors, presumably to prevent oxidation or corrosion of the copper conductors. However, the dielectric constant and thickness of the layer were not known; thus, the effect on measurements are unknown.

Figures 5.1 and 5.2 show the magnitude and phase plots of the experimental and calculated results. Note that agreement is good at lower frequencies (less than 2 GHz) and degrades somewhat as the frequency increases. The discrepancy can be attributed to the connectors. Time-domain reflectometry measurements were made, which confirmed the discontinuity introduced by the connectors.

A tapered three-line structure with the geometry shown in Figure 5.3 was measured. Except for the line length and line width, all other physical parameters are the same as those listed in Table 5.1. Figures 5.4 and 5.5 show the magnitude and phase of the transmission coefficient between ports 1 and 2 of the tapered three-line structure. The measured values agree reasonably well with the calculated values. Figures 5.6 and 5.7 show the magnitude and phase of the transmission coefficient between ports 2 and 5. The

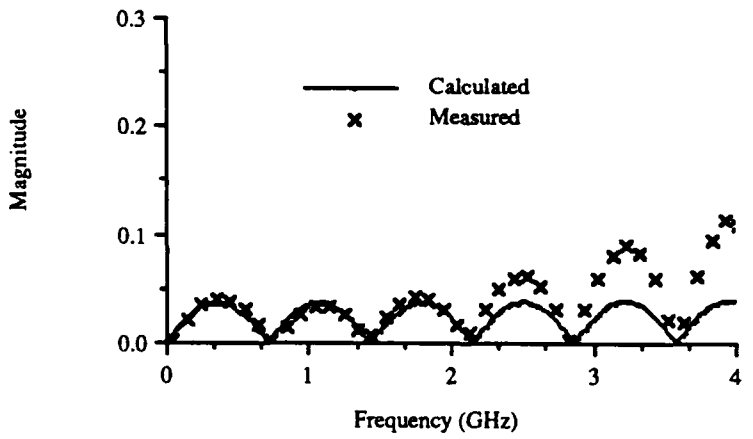

Figure 5.1. Calculated versus measured values of reflection coefficient magnitude for single uniform line.

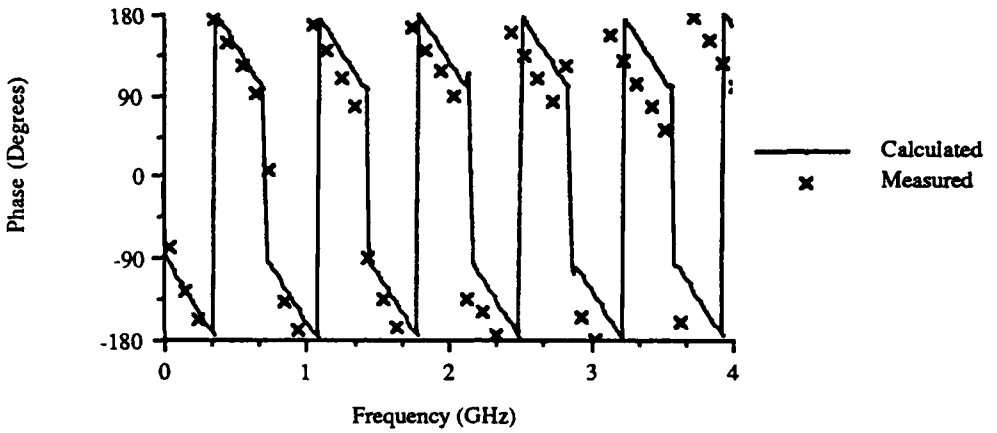

Figure 5.2. Calculated versus measured values of reflection coefficient phase for single uniform line.

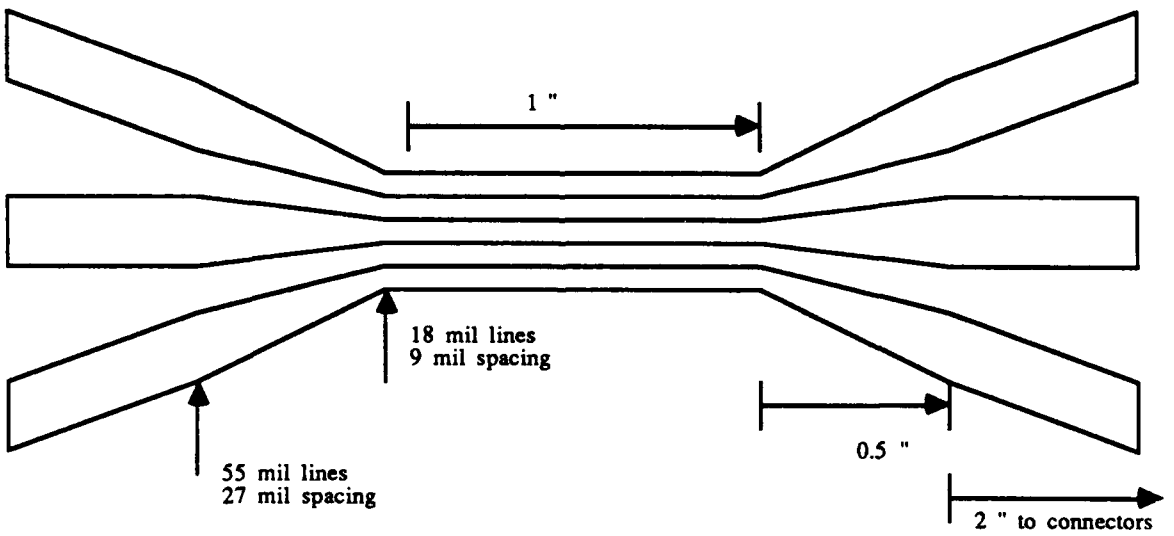

Figure 5.3. Three-line tapered geometry used for experimental measurements.

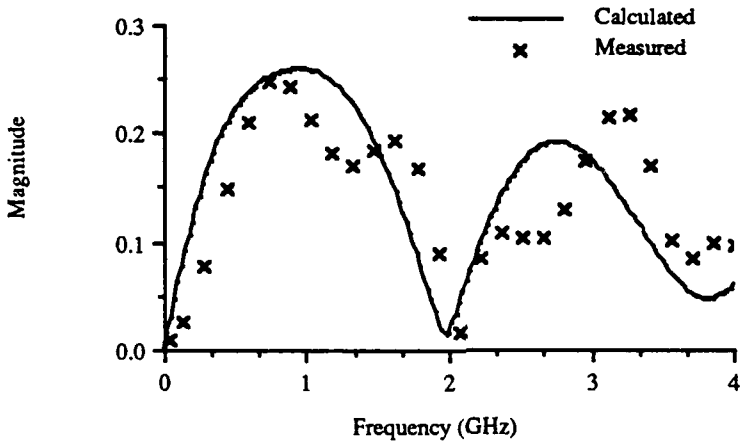

Figure 5.4. Calculated versus measured values for magnitude of S_{12} for coupled tapered lines.

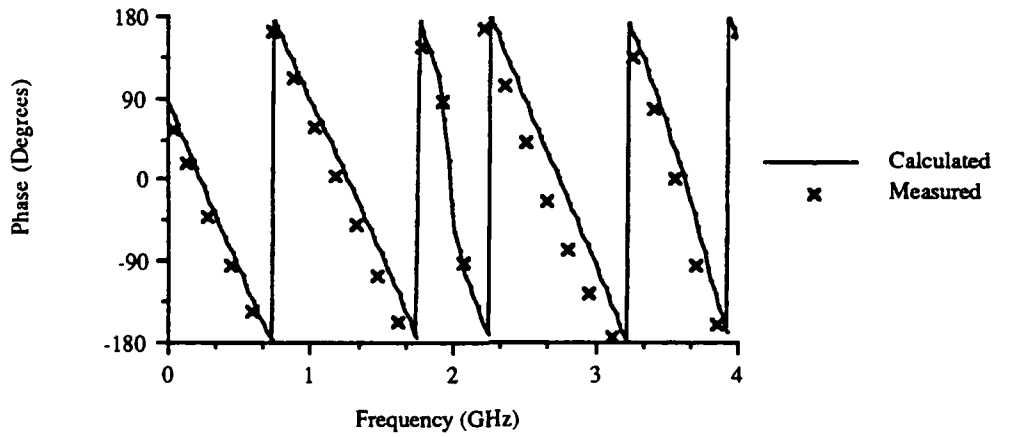

Figure 5.5. Calculated versus measured values for phase of S_{12} for coupled tapered lines.

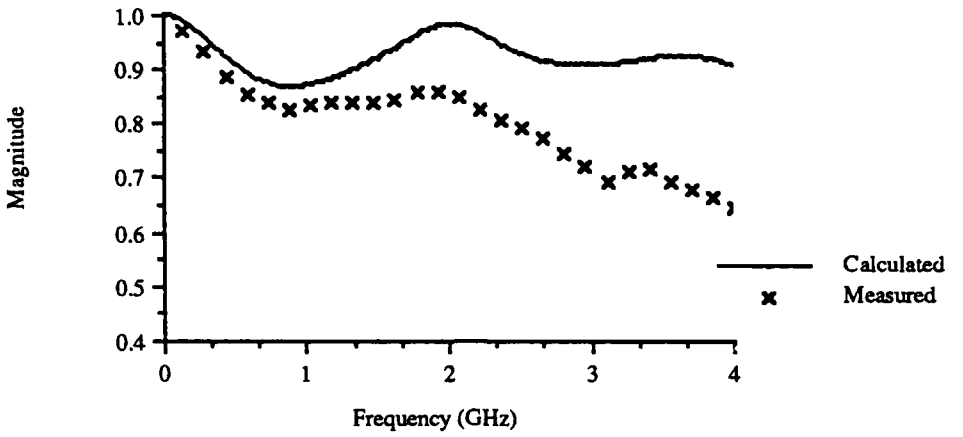

Figure 5.6. Calculated versus measured values for magnitude of S_{25} for coupled tapered lines.

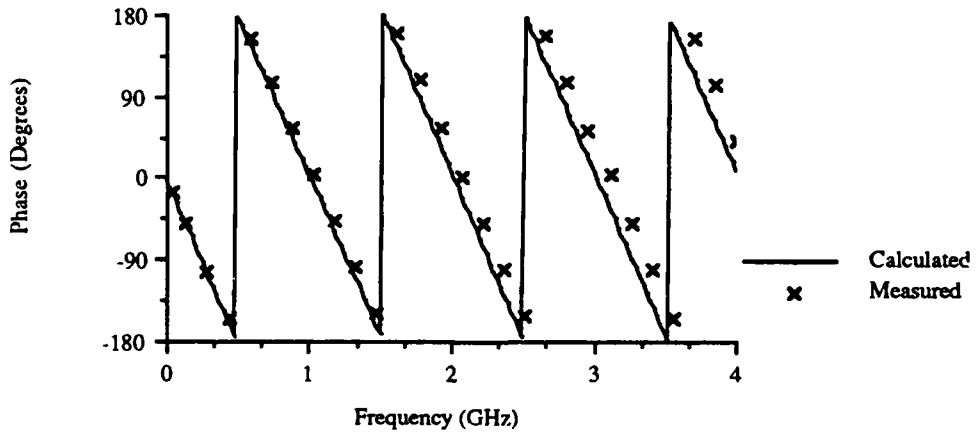

Figure 5.7. Calculated versus measured values for phase of S_{25} for coupled tapered lines.

phase agreement is good, but the measured magnitude values show more loss than the calculated values. This could be due to the fact that the calculated values do not include radiation loss or dielectric loss. These loss mechanisms become more important as the frequency increases, but can be neglected at lower frequencies. The model developed in this thesis does not include radiation loss, and the dielectric loss must be specified explicitly. Data for the dielectric loss were not available. However, the dielectric loss could be estimated from the experimental data.

To estimate the dielectric loss, the transmission coefficient magnitude data for the single uniform line was used. Figure 5.8 shows the experimental data along with the data calculated using only conductor loss. In order to match the experimental data, dielectric loss was added until the experimental and calculated curves agreed, as shown in Figure 5.8. Achieving this agreement required the following conductance matrix:

$$\mathbf{G} = 0.002\omega \begin{pmatrix} 1 & 0 & 0 \\ 0 & 1 & 0 \\ 0 & 0 & 1 \end{pmatrix}, \tag{5.1}$$

where ω is in gigaradians. Off-diagonal terms were tried, but were found to have little effect on the results.

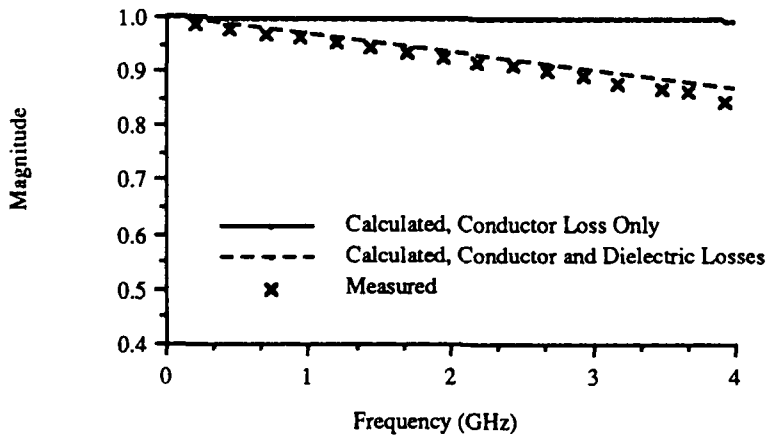

Figure 5.8. Calculated versus measured values of transmission coefficient magnitude for single uniform line, including dielectric loss.

The results of including the dielectric loss is shown in Figure 5.9. As can be seen, the calculated and measured data show better agreement than in Figure 5.6. Recall that Figure 5.6 includes only conductor loss, while Figure 5.9 includes both conductor and dielectric losses. The dielectric loss had little effect on any of the other data. Thus, for this particular substrate, which is supposed to be typical of printed circuit boards used in high-speed digital computers, dielectric loss has a greater effect on the transmission coefficient than conductor loss.

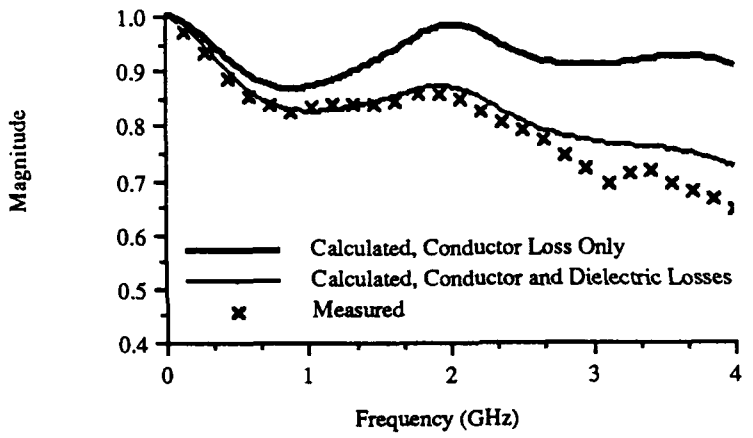

Figure 5.9. Calculated versus measured values for magnitude of S_{25} for coupled tapered lines, including dielectric loss.

5.4. Conclusions

In this chapter, comparisons were made between experimental measurements and values calculated using the technique described in previous chapters. Good agreement was found up to 4 GHz. At higher frequencies, the effects of the connectors became dominant, and comparisons between calculated and measured values could not be made. For a typical printed circuit board, dielectric loss could have a greater effect on the transmission coefficient than conductor loss.

CHAPTER 6.

EQUIVALENT CIRCUIT CHARACTERIZATION

6.1. Introduction

The equivalent circuit approach has been used for various microstrip discontinuities such as open ends, gaps, and step junctions. The practice of expressing a discontinuity in terms of an excess charge or current leads naturally to a lumped equivalent circuit. The use of equivalent circuits allows the designer to easily characterize the behavior of a circuit by simulation. The simulation time is much less when a discontinuity can be approximated as a lumped or transmission line circuit than when a full-wave analysis is performed. Also, lumped element or transmission line circuits can easily be integrated into most existing circuit simulators. However, no simple equivalent circuit has yet been proposed for a tapered line, perhaps because most analysis techniques require the discontinuity to be spatially localized.

Based on the S-parameters determined in Chapter 3, an equivalent circuit for coupled, tapered lines is proposed. The equivalent circuit is then tested by using it in a simulation program and comparing the time- and frequency-domain results with those of the full-scale simulation. The circuit model proposed here uses the idea that a taper can be viewed as a series of uniform transmission lines with step discontinuities. This allows the discontinuity to be spatially spread out, just as the original taper. Since the desired end result is a time-domain simulation, the step discontinuities themselves do not need to be modeled. The difference in impedance is sufficient for the time-domain simulator.

The equivalent circuit proposed in this chapter has both shortcomings and advantages. The major shortcoming is that the equivalent circuit is only good up to a particular frequency. However, analysis will show that if the equivalent circuit is chosen properly, the frequency will be high enough for an adequate time-domain simulation. The major advantage is its simplicity in implementation and simulation. As will be shown, it also does give reasonably good results for most digital pulses of current interest.

Discontinuities such as steps, gaps, and T-junctions have been widely studied and reported in the literature [10], [11], [14], [15], [45] - [51]. But the majority of these

approach the discontinuity as a localized phenomenon. However, Chu and Itoh did cascade two step junctions with good results [14]. This thesis extends that idea to the cascading of many step junctions to approximate a tapered line.

This chapter describes the development and testing of a simplified model for tapered, coupled lines. Section 6.2 describes the model used for the equivalent circuit. Empirical estimates of the equivalent circuit parameters are presented. Section 6.3 discusses the results of comparing the S-parameters of the model with previously derived S-parameters and time response for the tapered line. Finally, Section 6.4 presents some conclusions and observations related to the use of the equivalent circuit.

6.2 Model Development

Given the distributed nature of the tapered line discontinuity, no lumped equivalent circuit will model the line over a wide frequency range. Therefore, the choice was made to match the lower frequency characteristics. In the low-frequency limit, the taper should behave as if it was not there, leaving a junction with the load connected directly to the source. In the high-frequency limit, the entire structure should behave as if no discontinuity existed. A step junction equivalent circuit with frequency-dependent element values could model this behavior. However, no circuit simulator will accept frequency-dependent elements. Therefore, some simplification and approximation must be made. Since the fundamental frequency in a Fourier expansion of the digital pulse has the greatest magnitude, this frequency would be the most important to match. The fact that the Fourier coefficient magnitudes go to zero as the frequency increases allows the high-frequency asymptotic limit to be neglected.

As a result, the proposed circuit model is a combination of uniform transmission line sections, as shown in Figure 6.1. This model will supply both the periodic transmission line characteristics and the impedance matching characteristics of the tapered line. The total length of the uniform lines is the same as the length of the taper. The taper is divided into three sections, and each section is replaced by uniform coupled lines whose width and spacing equal the width and spacing at the midpoint of each section.

This model has a limited frequency range. The upper frequency limit is determined by the length of the taper and the frequency components of the input pulse. A common rule-of-thumb is that the equivalent circuit will be adequate up to the frequency at which the length of a section becomes a quarter wavelength. For a taper 7.874 cm long on a substrate

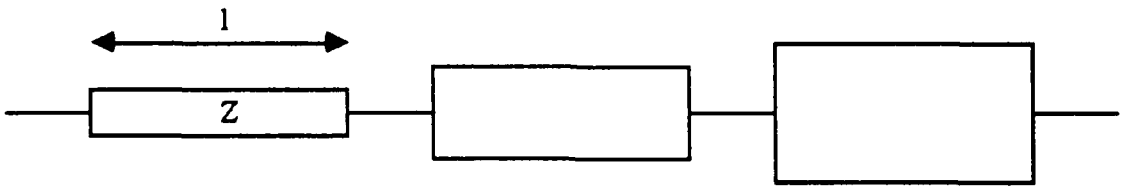

Figure 6.1. Symbolic equivalent circuit for a tapered line.

---

with relative dielectric constant 4.7, the frequency limit for a three-section equivalent circuit is given by

$$f = \frac{c}{\lambda\sqrt{\varepsilon_r}} \approx 1.7 \text{ GHz.} \tag{6.1}$$

This frequency limit will be compared with the actual results in the next section.

To determine the frequency range needed, a Fourier analysis of the input pulse can be performed. To simplify the analysis, two approximations will be made. The first is that the input pulse has zero rise time and fall time. The second is that any Fourier component whose magnitude is less than one-thousandth of the magnitude of the fundamental frequency can be neglected. These two assumptions will yield a worst-case estimate. The Fourier transform of a pulse is given by [52]

$$F\{\, \text{rect}(t) \,\} = \text{sinc}(f)\,, \tag{6.2}$$

where

$$\text{rect}(t) = \begin{array}{l} 1 \quad \text{for } |t| \le \frac{1}{2} \\ 0 \quad \text{for } |t| > \frac{1}{2} \end{array} \quad \text{and} \tag{6.3}$$

$$\text{sinc}(f) = \frac{\sin\pi f}{\pi f}. \tag{6.4}$$

If t is in nanoseconds, then f is in gigahertz. For a digital pulse with a period of 20 nsec, the fundamental frequency is 50 megahertz (MHz). The Fourier components become negligible at about 100 times the fundamental frequency, or 5 GHz. This number is on the same order of magnitude as the limit for the accuracy of the model. Thus, the model should give reasonable results. The results are presented in the next section.

6.3. Results

The S-parameters for the equivalent circuit developed in Section 6.2 were compared against those of the tapered line from which it was derived. The geometry for the structure is the same as used in Chapter 3 and listed in Table 3.3. Nonlinear terminations were used. The pulse parameters are the same as those used in Chapter 4 and listed in Table 4.2. The equivalent circuit consists of three sections of microstrip transmission line as described in the previous section. The frequency- and time-domain responses of both the tapered line and the equivalent circuit were calculated. Figures 6.2 through 6.5 show a comparison of the three-line equivalent circuit with the three-line taper.

As can be seen in the figures, the equivalent circuit data compare favorably with the full simulation data. In fact, if only the peak value of the crosstalk signal is desired and not the precise shape of the waveform, the equivalent circuit analysis is sufficient. The equivalent circuit calculation requires significantly less time than the full simulation. Execution time on an Apollo DN3500 workstation was about 135 sec for the equivalent circuit case, compared to 1593 sec for the full simulation case.

The reason for the close time-domain agreement can be seen in Figures 6.6 through 6.9. The plots are typical of all the S-parameters. Note that below 2 GHz the two curves in each figure agree closely. Since the Fourier components of the input pulse decay rapidly with frequency, the discrepancies in the S-parameters above 2 GHz have little effect on the propagated pulse. Note that the value observed in the graphs compares favorably with the value of 1.7 GHz determined in the previous section. However, some problems do arise around 3 GHz. Apparently, the equivalent circuit has some resonances at this frequency that do not exist in the original taper. However, since the input pulse has only negligible frequency components in this range, the effect of the resonance cannot be seen in the time-domain plots.

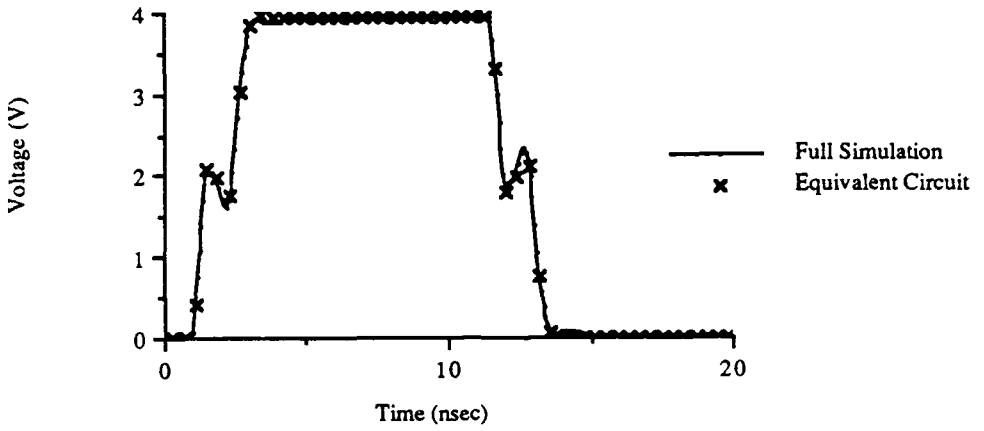

Figure 6.2. Near-end driven line time-domain response for coupled tapered lines.

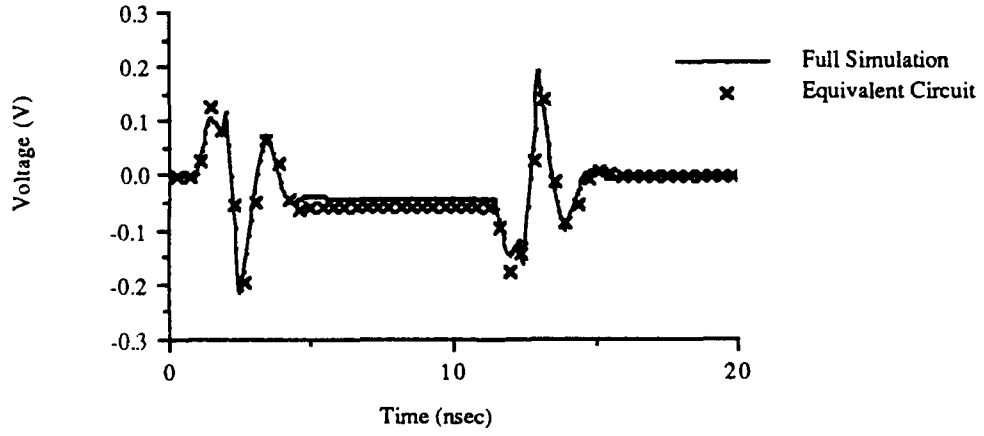

Figure 6.3. Near-end coupled line time-domain response for coupled tapered lines.

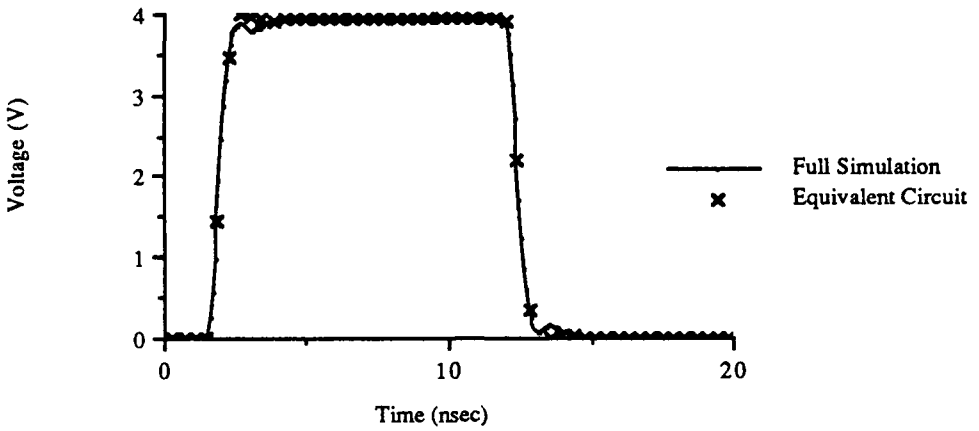

Figure 6.4. Far-end driven line time-domain response for coupled tapered lines.

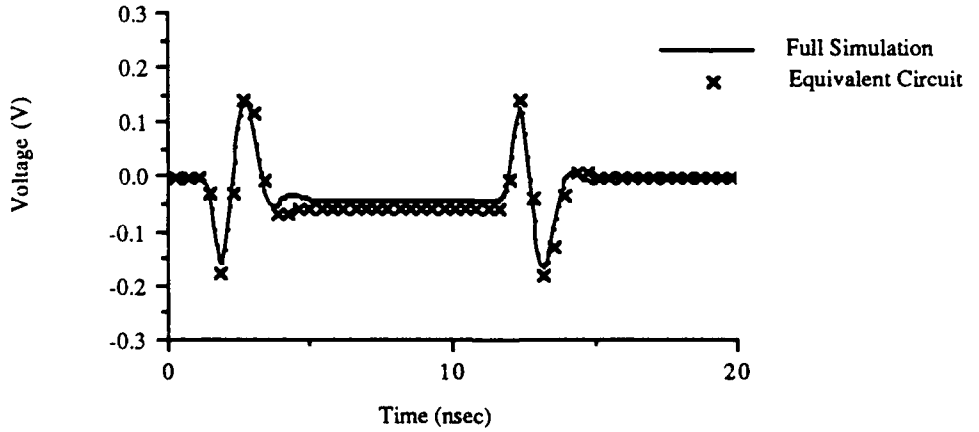

Figure 6.5. Far-end coupled line time-domain response for coupled tapered lines.

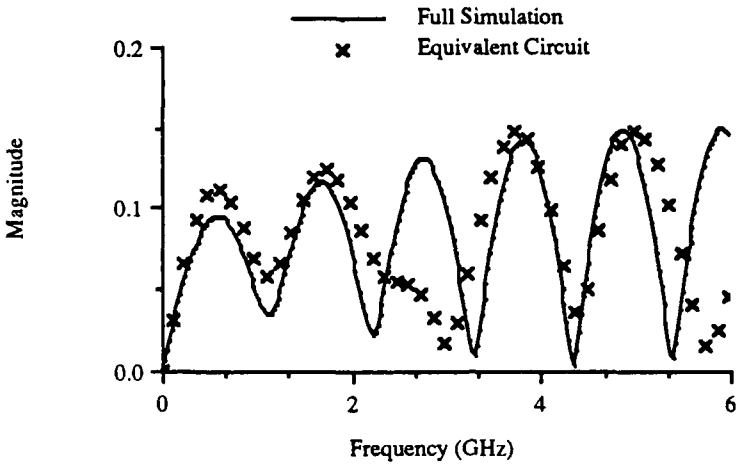

Figure 6.6. S_{22} magnitude for full simulation and equivalent circuit.

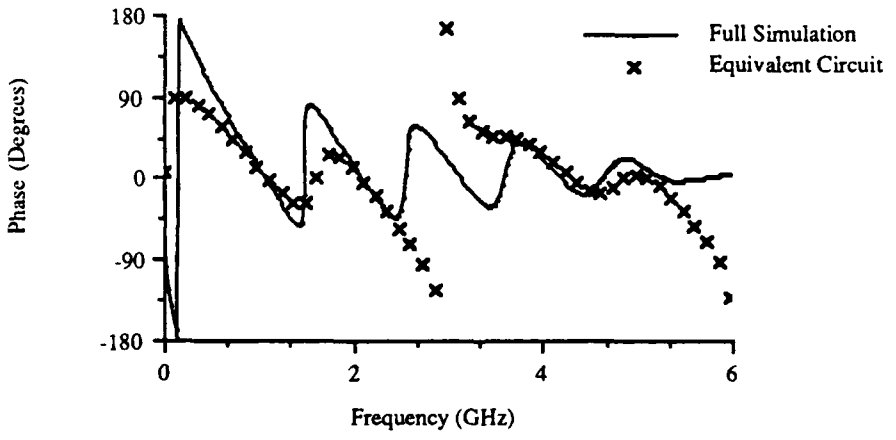

Figure 6.7. S_{22} phase for full simulation and equivalent circuit.

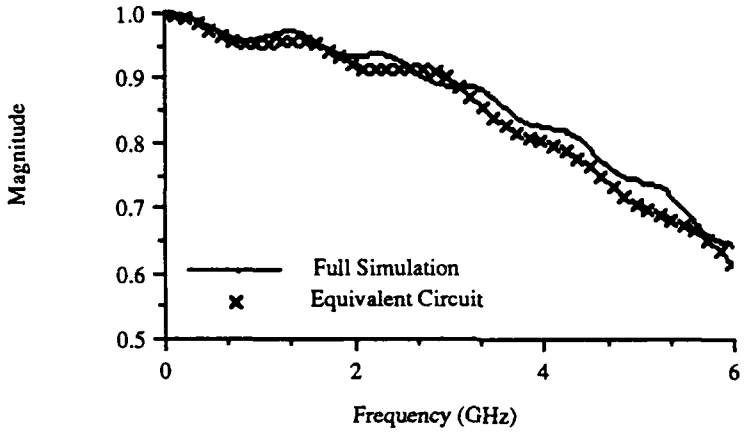

Figure 6.8. S_{25} magnitude for full simulation and equivalent circuit.

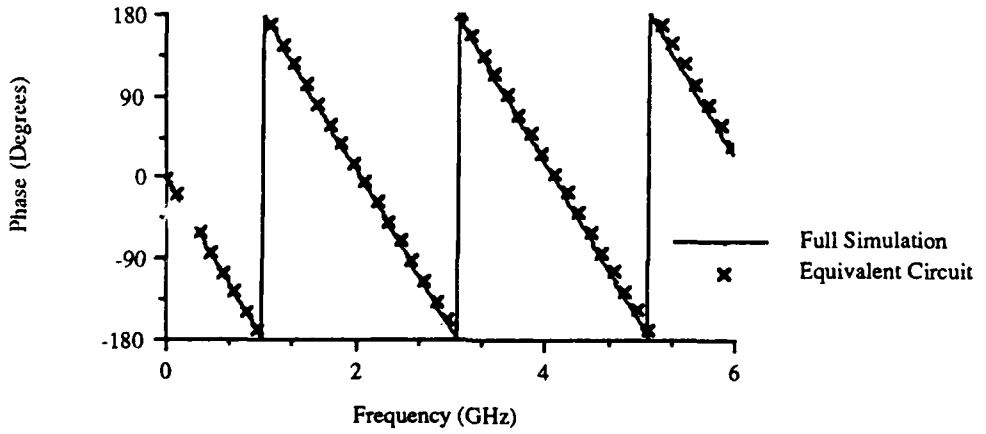

Figure 6.9. S_{25} phase for full simulation and equivalent circuit.

The proposed equivalent circuit was further tested by comparing the S-parameters against the S-parameters generated by the program Touchstone. However, since Touchstone cannot analyze coupled tapered lines, only results for a single tapered line will be compared. The parameters for the equivalent circuit are the same as used in Chapter 2 and listed in Table 2.1. Figures 6.10 through 6.13 show the results for the equivalent circuit and the tapered line as determined by Touchstone. Note that the curves agree well for frequencies up to 5 GHz. Above 5 GHz, the assumptions explained in Section 6.2 are no longer valid, and thus the curves do not agree as well.

6.4. Conclusions

In this chapter, an equivalent circuit for coupled, tapered microstrip lines has been proposed and tested. The equivalent circuit is valid over the frequency range of interest when excited by typical high-speed digital pulses. The time-domain responses of the equivalent circuit show good agreement with the response of the tapered line. Use of the equivalent circuit will reduce simulation time with a negligible effect on the accuracy of the results.

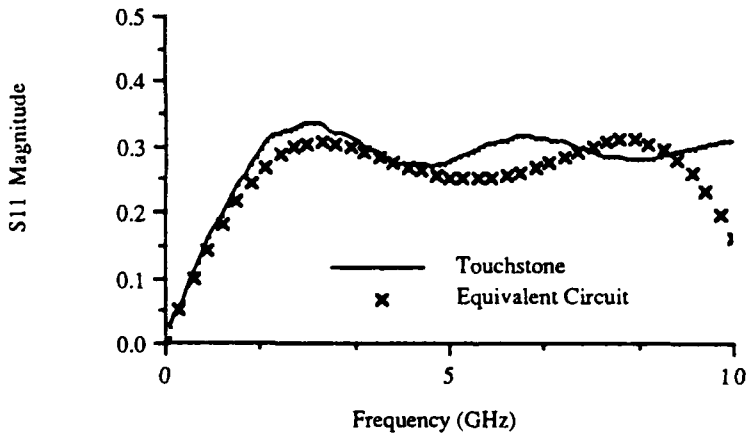

Figure 6.10. Reflection coefficient magnitude comparison between Touchstone and equivalent circuit.

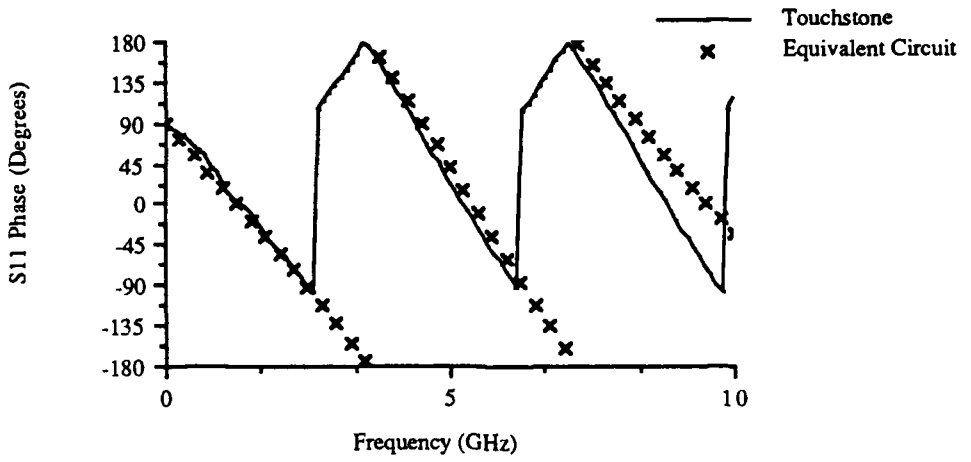

Figure 6.11. Reflection coefficient phase comparison between Touchstone and equivalent circuit.

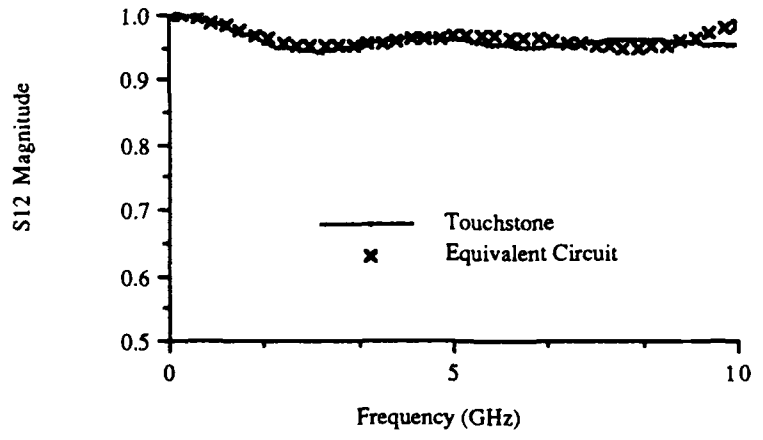

Figure 6.12. Transmission coefficient magnitude comparison between Touchstone and equivalent circuit.

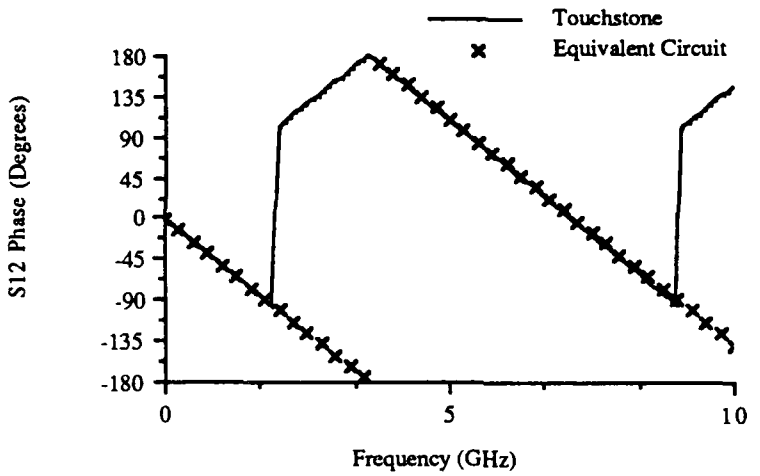

Figure 6.13. Transmission coefficient phase comparison between Touchstone and equivalent circuit.

CHAPTER 7.

CONCLUSIONS

In this thesis, a technique was described for analyzing multiple, tapered, microstrip lines as used for interconnects in high-speed digital circuits. First, the theory was developed and tested for single tapered lines, and then it was extended to multiple tapered lines. The theory uses an integral equation formulation to calculate the quasi-static characteristics of the lines and an iteration-perturbation approach based on potential theory to include dispersive effects caused by transverse currents. In addition, conductor losses and thickness were included. The S-parameters for the microstrip structures were calculated, and comparisons were made with results by other methods. Good agreement was found between this technique and other techniques.

A method of analyzing digital pulse propagation through multiple tapered microstrip lines terminated with nonlinear loads was described. In this method, the frequency-domain S-parameters are inverse Fourier transformed into a time-domain Green's function for the structure. The Green's function is convolved with the input pulse, and a Newton-Raphson algorithm is applied to the characteristics of the terminations to include the effects of the nonlinearities. Again, the results were compared with previously published results, and agreement was good. To confirm the validity of the technique, the calculated results were compared with experimental results. Measurements were taken to determine the S-parameters of a microstrip structure, and the calculated values showed good agreement with the measured values.

Finally, an equivalent circuit was proposed for a multiple tapered line structure. The equivalent circuit does not take the form of lumped elements because a taper is not a localized discontinuity that lends itself to modeling by lumped elements. Instead, the equivalent circuit is a minimum number of cascaded steps that yields the same time-domain response and the same frequency-domain response up to a given frequency as does the original tapered line. This form of an equivalent circuit is practical because most circuit simulators already have models for uniform lines and, thus, can easily be made to simulate tapered lines.

REFERENCES

[1] T. Itoh and R. Mittra, "Spectral-domain approach for calculating the dispersion characteristics of microstrip lines," *IEEE Trans. Microwave Theory Tech.*,vol. MTT-21, pp. 496-499, July 1973.

[2] M. Kobayashi and F. Ando, "Dispersion characteristics of open microstrip lines," *IEEE Trans. Microwave Theory Tech.*,vol. MTT-35, pp. 101-105, Feb. 1987.

[3] C. Chan and R. Mittra, "Spectral iterative technique for analyzing multiconductor microstrip lines," *IEEE MTT-S Digest*, pp. 463-465, 1984.

[4] B. E. Kretch and R. E. Collin, "Microstrip dispersion including anisotropic substrates," *IEEE Trans. Microwave Theory Tech.*, vol. MTT-35, pp. 710-718, Aug. 1987.

[5] K. N. S. Rao, V. Mahadevan, and S. P. Kosta, "Analysis of straight tapered microstrip transmission lines - ASTMIC," *IEEE Trans. Microwave Theory Tech.*, vol. MTT-25, p. 164, Feb. 1977.

[6] D. M. Syahkal and J. B. Davies, "Accurate analysis of tapered planar transmission lines for microwave integrated circuits," *IEEE Trans. Microwave Theory Tech.*,vol. MTT-29, pp. 123-128, Feb. 1981.

[7] W. R. Smith and D. E. Snyder, "Circuit loading and crosstalk signals from capacitance in SOS and bulk-silicon interconnect channels," *IEEE V-MIC Conference Proceedings*, pp. 218-227, 1984.

[8] G. Ghione, I. Maio, and G. Vecchi, "Modeling of multiconductor buses and analysis of crosstalk, propagation delay, and pulse distortion in high-speed GaAs logic circuits," *IEEE Trans. Microwave Theory Tech.*, vol. MTT-37, pp. 445-456, Mar. 1989.

[9] F. Romeo and M. Santomauro, "Time-domain simulation of n coupled transmission lines," *IEEE Trans. Microwave Theory Tech.*, vol. MTT-35, pp. 131-137, Feb. 1987.

[10] K. C. Gupta, R. Garg, and I. J. Bahl, *Microstrip Lines and Slotlines*. Norwood, MA: Artech House, 1979.

[11] E. A. Wolff and R. Kaul, *Microwave Engineering and System Applications*. New York, NY: John Wiley & Sons, 1988.

[12] Y. T. Lo and S. W. Lee, Eds., *Antenna Handbook*. New York, NY: Van Nostrand Reinhold Company, 1988.

[13] K. W. Goossen and R. B. Hammond, "Modeling of picosecond pulse propagation in microstrip interconnections on integrated circuits," *IEEE Trans. Microwave Theory Tech.*, vol. MTT-37, pp. 469-478, Mar. 1989.

[14] T. S. Chu and T. Itoh, "Generalized scattering matrix method for analysis of cascaded and offset microstrip step discontinuities," *IEEE Trans. Microwave Theory Tech.*, vol. MTT-34, pp. 280-284, Feb. 1986.

[15] B. M. Neale and A. Gopinath, "Microstrip discontinuity inductances," *IEEE Trans. Microwave Theory Tech.*, vol. MTT-26, pp. 827-831, Oct. 1978.

[16] R. E. Diaz, "The discrete variational conformal technique for the calculation of strip transmission-line parameters," *IEEE Trans. Microwave Theory Tech.*, vol. MTT-34, pp. 714-722, June 1986.

[17] E. G. Farr, C. H. Chan, and R. Mittra, "A frequency-dependent coupled-mode analysis of multiconductor microstrip lines with application to VLSI interconnection problems," *IEEE Trans. Microwave Theory Tech.*, vol. MTT-34, pp. 307-310, Feb. 1986.

[18] R. Garg and I. J. Bahl, "Characteristics of coupled microstriplines," *IEEE Trans. Microwave Theory Tech.*, vol. MTT-27, pp. 700-705, July 1979.

[19] K. D. Marx, "Propagation modes, equivalent circuits, and characteristic terminations for multiconductor transmission lines with inhomogeneous dielectrics," *IEEE Trans. Microwave Theory Tech.*, vol. MTT-21, pp. 450-457, July 1973.

[20] A. Sawicki and K. Sachse, "Lower and upper bound calculations on the capacitance of multiconductor printed transmission line using the spectral-domain approach and variational method," *IEEE Trans. Microwave Theory Tech.*, vol. MTT-34, pp. 236-244, Feb. 1986.

[21] S. D. Shamasundara and N. Singh, "Design of coupled microstrip lines," *IEEE Trans. Microwave Theory Tech.*, vol. MTT-25, pp. 232-233, Mar. 1977.

[22] V. K. Tripathi, "On the analysis of symmetrical three-line microstrip circuits," *IEEE Trans. Microwave Theory Tech.*, vol. MTT-25, pp. 726-729, Sep. 1977.

[23] V. K. Tripathi, "A dispersion model for coupled microstrips," *IEEE Trans. Microwave Theory Tech.*, vol. MTT-34, pp. 66-71, Jan. 1986.

[24] N. G. Alexopoulos and C. M. Krowne, "Characteristics of single and coupled microstrips on anisotropic substrates," *IEEE Trans. Microwave Theory Tech.*, vol. MTT-26, pp. 387-393, June 1978.

[25] E. Yamashita and K. Atsuki, "Analysis of microstrip-like transmission lines by nonuniform discretization of integral equations," *IEEE Trans. Microwave Theory Tech.*, vol. MTT-24, pp. 195-200, Apr. 1976.

[26] A. Nakatani and N. G. Alexopoulos, "Toward a generalized algorithm for the modeling of the dispersive properties of integrated circuit structures on anisotropic substrates," *IEEE Trans. Microwave Theory Tech.*, vol. MTT-33, pp. 1436-1441, Dec. 1985.

[27] B. E. Speilman, "Dissipation loss effects in isolated and coupled transmission lines," *IEEE Trans. Microwave Theory Tech.*, vol. MTT-25, pp. 648-656, Aug. 1977.

[28] T. G. Bryant and J. A. Weiss, "Parameters of microstrip transmission lines and coupled pairs of microstrip lines," *IEEE Trans. Microwave Theory Tech.*, vol. MTT-16, pp. 1021-1027, Dec. 1968.

[29] V. K. Tripathi, "Asymmetric coupled transmission lines in an inhomogeneous medium," *IEEE Trans. Microwave Theory Tech.*, vol. MTT-23, pp. 734-739, Sep. 1975.

[30] L. Su, T. Itoh, and J. Rivera, "Design of an overlay directional coupler by a full-wave analysis," *IEEE Trans. Microwave Theory Tech.*, vol. MTT-31, pp. 1017-1022 Dec., 1983.

[31] T. Kitazawa and Y. Hayashi, "Propagation characteristics of striplines with multilayered anisotropic media," *IEEE Trans. Microwave Theory Tech.*, vol. MTT-31, pp. 429-433, June 1983.

[32] M. Kirschning and R. H. Jansen, "Accurate wide-range design equations for the frequency-dependent characteristic of parallel coupled microstrip lines," *IEEE Trans. Microwave Theory Tech.*, vol. MTT-32, pp. 83-90, Jan. 1984.

[33] H. A. Wheeler, "Transmission line properties of parallel strips separated by a dielectric sheet," *IEEE Trans. Microwave Theory Tech.*, vol. MTT-13, pp. 172-175, Mar. 1965.

[34] R. A. Pucel, D. J. Masse, and C. P. Hartwig, "Losses in microstrip," *IEEE Trans. Microwave Theory Tech.*, vol. MTT-16, pp. 342-350, June 1968.

[35] H. A. Wheeler, "Transmission-line properties of a strip on a dielectric sheet on a plane," *IEEE Trans. Microwave Theory Tech.*, vol. MTT-25, pp. 631-647, Aug. 1977.

[36] E. Hammarstad and O. Jensen, "Accurate models for microstrip computer-aided design," *IEEE Microwave Symposium*, pp. 407-409, 1980.

[37] William H. Hayt, Jr., *Engineering Electromagnetics*. New York, NY: McGraw-Hill, 1974.

[38] H. A. Wheeler, "Formulas for the skin effect," *Proc. IRE, vol. 30*, pp. 412-424, 1942.

[39] M. V. Schneider, "Microstrip lines for microwave integrated circuits," *B. S. T. J., vol. 48*, pp. 1422-1444, May-June 1969.

[40] J. E. Schutt-Aine, "Modeling and simulation of high-speed digital circuit interconnections," Ph.D. dissertation, Electromagnetic Communication Laboratory, University of Illinois, Urbana, IL, 1988.

[41] G. Hasnain, A. Dienes, and J. R. Whinnery, "Dispersion of picosecond pulses in coplanar transmission lines," *IEEE Trans. Microwave Theory Tech.*, vol. MTT-34, pp. 738-741, June 1986.

[42] J. L. Hill and D Mathews, "Transient analysis of systems with exponential transmission lines," *IEEE Trans. Microwave Theory Tech.*, vol. MTT-25, pp. 777-783, Sep. 1987.

[43] L. O. Chua and P. M. Lin, *Computer-Aided Analysis of Electronic Circuits: Algorithms and Computational Techniques*. Englewood Cliffs, NJ: Prentice-Hall, Inc., 1975.

[44] D. A. Hodges and H. G. Jackson, *Analysis and Design of Digital Integrated Circuits*. New York, NY: McGraw-Hill, Inc., 1988.

[45] A. Gopinath and C. Gupta, "Capacitance parameters of discontinuities in microstriplines," *IEEE Trans. Microwave Theory Tech.*, vol. MTT-26, pp. 831-836, Oct. 1978.

[46] W. Menzel and I. Wolff, "A method for calculating the frequency-dependent properties of microstrip discontinuities," *IEEE Trans. Microwave Theory Tech.*, vol. MTT-25, pp. 107-112, Feb. 1977.

[47] R. H. Jansen, "Hybrid mode analysis of end effects of planar microwave and millimetrewave transmission lines," *IEE Proceedings*, vol. 128, pp. 77-86, Apr. 1981.

[48] P. B. Katehi and N. G. Alexopoulos, "Frequency-dependent characteristics of microstrip discontinuities in millimeter-wave integrated circuits," *IEEE Trans. Microwave Theory Tech.*, vol. MTT-33, pp. 1029-1035, Oct. 1985.

[49] R. W. Jackson and D. M. Pozar, "Full-wave analysis of microstrip open-end and gap discontinuities," *IEEE Trans. Microwave Theory Tech.*, vol. MTT-33, pp. 1036-1042, Oct. 1985.

[50] P. Benedek and P. Silvester, "Equivalent capacitances for microstrip gaps and bends," *IEEE Trans. Microwave Theory Tech.*, vol. MTT-20, pp. 729-733, Nov. 1972.

[51] C. J. Railton and T. Rozzi, "The rigorous analysis of cascaded step discontinuities in microstrip," *IEEE Trans. Microwave Theory Tech.*, vol. MTT-36, pp. 1177-1185, July 1988.

[52] G. R. Cooper and C. D. McGillem, *Modern Communications and Spread Spectrum*. New York, NY: McGraw-Hill, Inc., 1986.

VITA

Mark Andrew Mehalic [redacted] He attended Derry Area High School in Derry, Pennsylvania, and entered the Pennsylvania State University in September, 1976. In May 1980, he was graduated with a Bachelor of Science degree in Electrical Engineering and was commissioned as a Second Lieutenant in the United States Air Force. He was then assigned to the Air Force Wright Aeronautical Laboratories, Wright-Patterson Air Force Base, Ohio, where he was involved in the design and development of digital flight control systems. In June 1982, he entered graduate school at the Air Force Institute of Technology. He received a Master of Science degree in Electrical Engineering and was assigned to the Electronic Warfare Division of the 3246th Test Wing, Eglin Air Force Base, Florida, where he worked as a test engineer and eventually as Test Director for various electronic warfare flight test programs. In September 1986, he entered graduate school at the University of Illinois. For the next three years, he performed research in the High-Speed Digital Circuits Group of the Electromagnetic Communication Laboratory. He is a member of Eta Kappa Nu and Tau Beta Pi, and is author/coauthor of the following journal article and conference proceedings:

M. Mehalic, "Effects of computer architecture on DFT algorithm performance," *NAECON 84 Digest, vol. 1*, pp. 54 - 61, 1984.

M. Mehalic, P. Rustan, and G. Route, "Effects of architecture implementation on DFT algorithm performance," *IEEE Trans. Acous., Speech, Signal Processing*, pp. 684-693, June 1985.

M. Mehalic, C. Chan, and R. Mittra, "Investigation of tapered multiple microstrip lines for VLSI circuits," *IEEE MTT-S International Microwave Symposium Digest*, pp. 215-218, 1988.